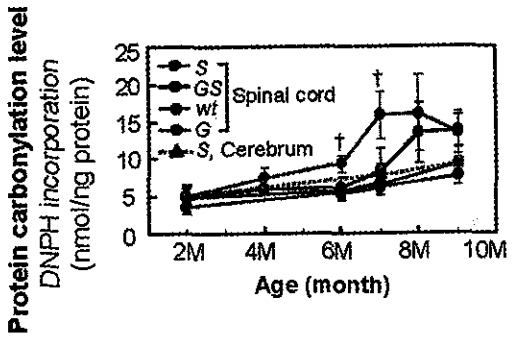

Figure 6. Oxidative modification of proteins is slowly increased by GluR2 overexpression. Tissue extracts were treated with DNPH, which specifically reacted with carbonyl groups in the protein side chains and converted into DNP–hydrazone. The levels of carbonylated proteins in spinal cords, which were evaluated from the absorption of DNP–hydrazone (375 nm), were significantly higher in the 6- and 7-month-old S littermates and 8-month-old GS littermates compared with G and wt littermates ($P < 0.05$). In comparison between the S and GS littermates, the carbonylated protein levels were significantly higher in S than GS littermates at the age of 6 and 7 months († $P < 0.05$). $n = 3$–4 mice per each group.

Ca^{2+}-influx though motoneuronal AMPA receptors promotes conversion of SOD1 protein into aberrant forms

In addition to delaying the disease onset, GluR2 overexpression succeeded in delaying the conversion of SOD1 protein into unusual forms (Figs 4 and 5B). To date, more than 20 papers have reported the delay of disease onset in mutant SOD1 transgenic mice by various pharmacological or transgenic techniques (1). However, the effects of such trials on SOD1 conformational changes have yet to be shown. Here, we provide the first evidence that disease onset is delayed when conversion of SOD1 into unusual forms is delayed, consistent with the hypothesis that SOD1 aggregation participates in ALS pathogenesis.

This study also provides an outline of the temporal profile for the formation of unusual SOD1 species during the clinical course of mouse ALS. Previous studies with western blots detected two distinct patterns of unusual SOD1 species in spinal cord extracts from mutant SOD1 transgenic mice. One is a set of oligomer-sized species (9), and another contains species between a monomer and dimer in size (10–12). Here, we show that trimer- and tetramer-sized species are detectable in the post-mitochondrial fractions containing cytosolic proteins (Fig. 4A), whereas species between a monomer and dimer in size are detected in the crude mitochondrial fractions containing major cellular components such as organelles and cytoskeleton. On the other hand, dimer-sized species were detectable in both fractions (Figs 4B and 5B). The amount of trimer and tetramer-sized species in the cytosol seemed comparatively very small to the unusual species in the organelle/cytoskeleton fractions, as these species are no longer detectable in Figure 5B, an experiment in which the same subcellular fraction amounts were loaded to the respective lanes. The first detectable unusual SOD1 species are dimer-sized species that appear several months before disease onset. Subsequently, a very small population of SOD1 proteins grows into trimer- and tetramer-sized species in the cytosol. On the other hand, a large amount of SOD1 protein is converted into ~25 and 35 kDa-sized species. These unusual species first appear in the P1 and P2 fractions and then extensively accumulate into the P1 fraction by disease onset. The presence in the P2 mitochondrial fraction might be related to the dysfunction of mitochondria that has been reported in $hSOD1^{G93A}$ mice around disease onset (1,31). In the P1 fraction, nuclei and certain kind of filamentous cytoskeletons such as neurofilaments and GFAP, but not actin filaments or microtubiles, are effectively concentrated. The extensive accumulation of unusual SOD1 species in the P1 fraction implies that these species are fundamentally associated with neurofilaments or GFAP, because a further fractionation study revealed that these species do not independently accumulate in the nuclei (data not shown). Abnormalities in the neurofilaments observed in ALS patients and mutant SOD1 mice, such as an accumulation of neurofilament inclusions (1) and a defect in axonal transport (4), might be closely related to this phenomenon. Alternatively, those SOD1 species might be involved in aggresome-like structures, as observed in HEK293 cells transfected with G85R and G93A SOD1 mutants (9). After disease onset, unusual species spread to other organelle fractions enriched in lysosomes, peroxysomes and microsomes derived from the endoplasmic reticulum (ER), Golgi apparatus and plasma membrane. These alterations in SOD1 proteins are thought to predominantly occur in motoneurons and surrounding astrocytes, as SOD1-containing proteinacious inclusions, which are likely to have developed from high-molecular-weight-shifted SOD1 species, are specifically detected in motoneurons and neighboring astrocytes in end-stage $hSOD1^{G93A}$ mice (6–8). The reduction of Ca^{2+}-influx through motoneuronal AMPA receptors successfully delayed the formation of the entire range of unusual SOD1 species in the spinal cord extracts (Figs 4 and 5A) as well as the development of astrogliosis (Fig. 3C). These results suggest that Ca^{2+}-influx through motoneuronal AMPA receptors can affect the physiology of neighboring astrocytes as well as their own, and contributes to the misfolding and subsequent conversion of SOD1 protein.

Ca^{2+}-influx through AMPA receptors enhances ROS production, which may induce the misfolding of SOD1 proteins

Ca^{2+}-influx through motoneuronal AMPA receptors seems to enhance oxidative stress primarily in motoneurons and secondarily in neighboring astrocytes. Activation of Ca^{2+}-permeable AMPA receptors causes rapid increases in the level of cytosolic calcium, which are rapidly attenuated by trapping with Ca^{2+}-chelating proteins and by incorporation of calcium into mitochondria and ER (40). As spinal motoneurons are less capable of buffering increased calcium levels, probably due to a lack of major Ca^{2+}-chelating proteins such as parvalbumin and calbindin D28K (41), a large proportion of free calcium is reported to be incorporated into mitochondria, resulting in enhanced ROS production (42). Evidence suggests that ROS generated in motoneurons can exit from the motoneurons and cause oxidative disruption of glutamate transporters and increased ROS level in neighboring

astrocytes (43). The loss of astrocytic glutamate transporters, which has been preferentially observed in the affected area in ALS patients and mouse models (15,43,44), accelerates AMPA receptor-mediated Ca^{2+}-influx and ROS generation within motoneurons, resulting in a vicious cycle to enhance the oxidative stress in motoneurons and neighboring astrocytes (45).

Enhanced ROS levels might, in part, account for the formation of unusual SOD1 species, as oxidative modification by ROS has been shown to convert SOD1 proteins into a variety of unusual forms, at least *in vitro* (34,35). We found a good correlation between the levels of carbonylated proteins and unusual SOD1 species in the spinal cord extracts from S and GS mice. Both levels were rapidly increased at disease onset, but these increases were similarly attenuated when the Ca^{2+}-permeability of AMPA receptors was reduced (Figs 4, 5B and 6). This correlation may imply that the increased cellular oxidative stress resulting from activation of motoneuronal Ca^{2+}-permeable AMPA receptors induces the misfolding and subsequent conversion of SOD1 protein within motoneurons and adjacent glial cells.

MATERIALS AND METHODS

The sequence information for the primers and probes is described in Supplementary Material, Table S1. All the data shown are representative of three mice per group when the number of mice (n) used for experiments is not mentioned. Signals in immunoblots and RT–PCR were quantified with NIH image software (1.61J). Statistical significance was assessed by the two-tailed Student's t-test when the statistical method is not mentioned. All protein electrophoreses in this paper utilized SDS–PAGE under reducing conditions. Antibodies were used for immunoblots and immunohistochemistry, which comprised of: anti-SOD1 (Stressgen, SOD-100), anti-GluR2 (BD PharMingen, 556341), anti-ChAT (Chemicon, AB144P), anti-cytochrome *c* (BD PharMingen, 556433), anti-Hsp60 (Sigma, H4149), anti-actin (Chemicon, MAB1501), anti-GFAP (Chemicon, MsX GFAP), anti-prohibitin (NeoMarkers, MS-261-P0), anti-CoxIV (Molecular Probes, A-6431), anti-nucleoporin p62 (BD Transduction Laboratories, N43620), anti-ribophorin I (Santa Cruz, sc-12164), anti-Lamp1 (BD PharMingen, 553792), anti-adaptin gamma (BD Transduction Laboratories, A36120), anti-neurofilament-M (Chemicon, AB1987), and anti-beta-tubulin (Sigma, T 4026) antibodies.

Generation of GluR2 transgenic mice

The transgene construct contained the 6.4 kb promoter region of the mouse *ChAT* gene (AF019045), the 2.6 kb rat *GluR2* coding sequence (CDS, M85035), internal ribosome entry sequence (IRES), *EGFP* CDS and the SV40 polyadenylation signal, in that order. As the *ChAT* promoter region contains an open reading frame of a vesicular acetylcholine transporter (*VAChT*) intronless gene (23), we introduced a stop codon at the 55th amino acid position to avoid producing a functional VAChT protein from this construct. The region from *IRES* to the polyadenylation signal was derived from the pIRES2–EGFP vector (Clonetech), with a base substitution so as to delete a *Not*I site in the *EGFP* 3′-untranslated region. The *Not*I-digested 10.9 kb DNA fragment was injected into C57BL/6J mouse eggs, and three transgenic lines, Tg3, Tg7 and Tg10, were established.

Taqman quantitative DNA PCR was performed using probe–primer sets specific to *EGFP* and two internal control genes, *SOD1* and *CPTI*, on an ABI7700 thermal cycler (PE Biosystems) under the conditions recommended by the manufacturer. Data were normalized using results from the *EGFP* knock-in mouse in the *Cx43* gene (M. Tanaka and S. Itohara, unpublished data), which displays a single copy of *EGFP* in the genome. Then absolute *EGFP* copy numbers in Tg3 ($n = 3$) Tg7 ($n = 3$) and Tg10 ($n = 5$) of *chat-GluR2* mice were calculated as 2.10 ± 0.04, 9.31 ± 0.14 and 16.44 ± 0.67 copies for the *SOD1* control, and 2.13 ± 0.07, 10.20 ± 0.09 and 16.43 ± 1.28 copies for the *CPTI* control, respectively (mean $\pm$ SD). The transgene copy number was thus represented as the mean of these two values.

Electrophysiological recordings

Electrophysiological experiments were performed as previously described (46) using 200–250 μm slices of spinal cord lumbar regions from mice at the postnatal ages of 4–7 days. Whole-cell patch-clamp recordings were performed with motoneurons identified using biocytin-containing Cs-based intracellular solution. To isolate the AMPA current, the extracellular solution contained 20 μM bicuculline, 25 μM D-2-amino-phosphonovaleric acid (D-APV) and 10 μM strychnine, which blocks the GABA, NMDA and glycine receptors, respectively. A glass electrode containing artificial cerebrospinal fluid positioned in the spinal cord was used for synaptic stimulation.

Quantitative analysis of gene expression levels in motoneurons

Spinal cords from 6–8-month-old mice were dissected without fixation, immediately embedded in OCT compound (Tissue-Tek), and frozen in liquid nitrogen. Frozen sections 30 μm thick were processed and stained using 0.01% toluidine blue, and motoneurons in spinal cords were clipped out of sections using laser microdissection (AS LMD, Leica) according to the manufacturer's protocol. About 1000 clipped slices of motoneurons were collected per mouse and subjected to RNA purification using an RNAeasy kit (Qiagen), followed by cDNA synthesis primed with oligo-dT using Superscript II (Gibco-Brl). The gene expression level was examined by Taqman real-time quantitative PCR using probe–primer sets specific to target genes. PCR was performed on an ABI7700 thermalcycler (PE Biosystems) under the manufacturer's recommended conditions, using cDNA derived from 60 (for *GluR2-4* and *ChAT*) or 10 (for *SOD1* and *GAPDH*) clipped slices of motoneurons as templates. Data were normalized with the expression level of *GAPDH*, and presented as a relative expression level compared with the level in the C57BL/6J non-transgenic control mouse.

Animals

Non-transgenic littermates without any transgene are indicated as wt to distinguish them from non-transgenic control mice,

C57BL/6J mice. All data except for Table 1 and Figure 1E are comparisons among littermates. The G1L line of transgenic mice harboring the G93A-mutated human *SOD1* gene (*B6SJL-TgN(SOD1-G93A)*1Gur^{dl}) was purchased from Jackson Laboratories and backcrossed with C57BL/6J mice. We used the littermates generated by crossing male *hSOD1*^{G93A} mice (fourth backcross-generation) with female *chat-GluR2* transgenic mice for all analyses except for a study of disease onset and mortality in Tg10 line (Table 2 and Fig. 2B and C), that involved three S and three GS littermates generated from the third backcrossed *hSOD1*^{G93A} mouse. To determine the day of disease onset, mice were subjected to the rotarod test (47). The retention time on a rotating wheel, the rotarod score, was measured four times per day with a 1-week interval in a blind fashion. Each trial lasted for a maximum of 5 min, during which time the wheel rotates with a linear acceleration from 4 to 40 rpm. The day of disease onset was defined as the day just before the mean retention time of four trials was sequentially shortened to <80% of the previous time. The end time was defined as the day of death or the day when the mouse was unable to right itself within 30 s (25).

Preparation of crude mitochondrial and post-mitochondrial fractions

Crude mitochondrial and post-mitochondrial fractions were prepared according to an established method (31) with certain modifications. The bovine strum albumin concentration in buffer H was reduced to 0.1%. The spinal cord L1–L5 segments were homogenized in buffer H (1 mg tissue/10 μl buffer H) on ice and centrifuged at 600*g* for 5 min at 4°C to remove unbroken cells. The supernatant was centrifuged at 13 500*g* for 10 min at 4°C, dividing into pellet (crude mitochondrial fraction) and supernatant (post-mitochondrial fraction).

Size-exclusive chromatography

Approximately 200 μg of cytosolic extracts were filtered through Millex-HV PVDF filters (Millipore, 0.45 μm diameter), concentrated with a Vivaspin column (Vivascience, cut-off size, MW 10 000), then resolved on a Superdex200 PC3.2/30 column (linear fractionation range, MW 10 000–600 000; bed volume, 2.4 ml; Pharmacia Biotech) at a flow rate of 40 μl/min in 50 mM sodium phosphate with 150 mM NaCl, pH 7.0. Fractionation started when 800 μl was eluted, and a 30 μl/tube of elutant was collected for a total of 48 tubes. Void volume was determined by the elution profile of dextran blue (2000 kDa). The column was calibrated using gel filtration calibration kits for high- and low-molecular weights (Amersham Bioscience).

Subcellular fractionation

Figure 5A represents a schematic of this procedure. Whole spinal cords were gently homogenized in modified buffer H [0.22 M D-mannitol, 0.07 M sucrose, 20 mM HEPES, pH 7.4, 1 mM EGTA and complete protease inhibitor cocktail (Roche), at 1 mg tissue/10 μl buffer] with a glass–Teflon homogenizer (10 up-and-down strokes) on ice, and centrifuged at 600*g* for 10 min. The supernatants were sequentially centrifuged at 5000*g* for 15 min, 8000*g* for 15 min and 100 000*g* for 1 h, to obtain three pellets (P2, P3 and P4) and the resulting supernatant (S). The pellets generated by the first brief centrifugation were very gently suspended with 2.2 M sucrose containing complete protease inhibitor cocktail (1 mg starting tissue/15 μl), and centrifuged at 40 000*g* for 1 h. The resulting pellets (P1) were rinsed with modified buffer H followed by centrifugation at 12 000*g* for 10 min. The pellets of P1, P2, P3 and P4 were finally resuspended with 1/4, 2, 1/2 and 1/2 volume (μl) of modified buffer H per starting tissue weight (mg), respectively. All centrifugations were performed at 4°C.

Measurement of protein carbonylation

Freshly dissected tissues were sonicated in buffer [50 mM Tris–HCl, pH 7.6, 20 mM $Na_4P_2O_7$, 20 mM sodium fluoride, 1 mM EGTA, 5 mM EDTA, 5 mM DTT and complete protease inhibitor cocktail (Roche), at 1 mg tissue/20 μl buffer] and centrifuged at 500*g* for 5 min. The supernatants were further centrifuged at 100 000*g* for 1 h, and the resulting supernatants were used. The levels of carbonylated proteins in these supernatants were evaluated by measuring absorbance derived from dinitrophenyl (DNP)–hydrazone as previously described (36) with slight modifications. We started with 40 μg of protein and used 6% SOD for a solubilization of the trichloroacetic acid precipitates.

SUPPLEMENTARY MATERIAL

Supplementary Material is available at HMG Online.

ACKNOWLEDGEMENTS

We wish to thank Drs Shin Kwak and Hiroshi Funakoshi for critical reading of the manuscript, Pacific Edit and Ms Bonnie Lee La Madeleine for review prior to submission for publication, Drs Takashi Sakurai, Haruhisa Inoue, Yasuyuki Suzuki and Runa Araya for helpful suggestions, and Ms Sachiko Iita, Yoshie Yoshida (LMD sampling) and Tomoko Yoda (rotarod test) for technical supports. We would also like to thank Drs Stephen F. Heinemann and Yuzuru Imai for kindly donating rat GluR2-4 cDNAs and anti-ubiquitin antibody, respectively. This work was funded by research grants from RIKEN BSI, a Grant-in-Aid for Scientific Research on Priority Area (Advanced Brain Science Project) from the Ministry of Education, Culture, Sports, Science and Technology, Japan, and grants from the Ministry of Health, Labor and Welfare, Japan.

REFERENCES

1. Julien, J.P. (2001) Amyotrophic lateral sclerosis unfolding the toxicity of the misfolded. *Cell*, **104**, 581–591.
2. Rosen, D.R., Siddique, T., Patterson, D., Figlewicz, D.A., Sapp, P., Hentati, A., Donaldson, D., Goto, J., O'Regan, J.P., Deng, H.X. *et al.* (1993) Mutations in Cu/Zn superoxide dismutase gene are associated with familial amyotrophic lateral sclerosis. *Nature*, **362**, 59–62.

3. Gurney, M.E., Pu, H., Chiu, A.Y., Dal Canto, M.C., Polchow, C.Y., Alexander, D.D., Caliendo, J., Hentati, A., Kwon, Y.W., Deng, H.X. *et al.* (1994) Motor neuron degeneration in mice that express a human Cu,Zn superoxide dismutase mutation. *Science*, **264**, 1772–1775.
4. Cleveland, D.W. and Rothstein, J.D. (2001) From Charcot to Lou Gehrig: deciphering selective motor neuron death in ALS. *Nat. Rev. Neurosci.*, **2**, 806–819.
5. Valentine, J.S. and Hart, P.J. (2003) Misfolded CuZnSOD and amyotrophic lateral sclerosis. *Proc. Natl Acad. Sci. USA*, **100**, 3617–3622.
6. Shibata, N., Asayama, K., Hirano, A. and Kobayashi, M. (1996) Immunohistochemical study on superoxide dismutases in spinal cords from autopsied patients with amyotrophic lateral sclerosis. *Dev. Neurosci.*, **18**, 492–498.
7. Bruijn, L.I., Houseweart, M.K., Kato, S., Anderson, K.L., Anderson, S.D., Ohama, E., Reaume, A.G., Scott, R.W. and Cleveland, D.W. (1998) Aggregation and motor neuron toxicity of an ALS-linked SOD1 mutant independent from wild-type SOD1. *Science*, **281**, 1851–1854.
8. Watanabe, M., Dykes-Hoberg, M., Culotta, V.C., Price, D.L., Wong, P.C. and Rothstein, J.D. (2001) Histological evidence of protein aggregation in mutant SOD1 transgenic mice and in amyotrophic lateral sclerosis neural tissues. *Neurobiol. Dis.*, **8**, 933–941.
9. Johnston, J.A., Dalton, M.J., Gurney, M.E. and Kopito, R.R. (2000) Formation of high molecular weight complexes of mutant Cu, Zn-superoxide dismutase in a mouse model for familial amyotrophic lateral sclerosis. *Proc. Natl Acad. Sci. USA*, **97**, 12571–12576.
10. Wang, J., Xu, G. and Borchelt, D.R. (2002) High molecular weight complexes of mutant superoxide dismutase 1: age-dependent and tissue-specific accumulation. *Neurobiol. Dis.*, **9**, 139–248.
11. Wang, J., Slunt, H., Gonzales, V., Fromholt, D., Coonfield, M., Copeland, N.G., Jenkins, N.A. and Borchelt, D.R. (2003) Copper-binding-site-null SOD1 causes ALS in transgenic mice: aggregates of non-native SOD1 delineate a common feature. *Hum. Mol. Genet.*, **12**, 2753–2764.
12. Puttaparthi, K., Wojcik, C., Rajendran, B., DeMartino, G.N. and Elliott, J.L. (2003) Aggregate formation in the spinal cord of mutant SOD1 transgenic mice is reversible and mediated by proteasomes. *J. Neurochem.*, **87**, 851–860.
13. Durham, H.D., Roy, J., Dong, L. and Figlewicz, D.A. (1997) Aggregation of mutant Cu/Zn superoxide dismutase proteins in a culture model of ALS. *J. Neuropathol. Exp. Neurol.*, **56**, 523–530.
14. Shaw, P.J. and Eggett, C.J. (2000) Molecular factors underlying selective vulnerability of motor neurons to neurodegeneration in amyotrophic lateral sclerosis. *J. Neurol.*, **247** (Suppl. 1), I17–I27.
15. Rothstein, J.D., Van Kammen, M., Levey, A.I., Martin, L.J. and Kuncl, R.W. (1995) Selective loss of glial glutamate transporter GLT-1 in amyotrophic lateral sclerosis. *Ann. Neurol.*, **38**, 73–84.
16. Van Damme, P., Leyssen, M., Callewaert, G., Robberecht, W. and Van Den Bosch, L. (2003) The AMPA receptor antagonist NBQX prolongs survival in a transgenic mouse model of amyotrophic lateral sclerosis. *Neurosci. Lett.*, **343**, 81–84.
17. Gurney, M.E., Fleck, T.J., Himes, C.S. and Hall, E.D. (1998) Riluzole preserves motor function in a transgenic model of familial amyotrophic lateral sclerosis. *Neurology*, **50**, 62–66.
18. Bar-Peled, O., O'Brien, R.J., Morrison, J.H. and Rothstein, J.D. (1999) Cultured motor neurons possess calcium-permeable AMPA/kainate receptors. *Neuroreport*, **10**, 855–859.
19. Kruman, II, Pedersen, W.A., Springer, J.E. and Mattson, M.P. (1999) ALS-linked Cu/Zn-SOD mutation increases vulnerability of motor neurons to excitotoxicity by a mechanism involving increased oxidative stress and perturbed calcium homeostasis. *Exp. Neurol.*, **160**, 28–39.
20. Hollmann, M. and Heinemann, S. (1994) Cloned glutamate receptors. *Annu. Rev. Neurosci.*, **17**, 31–108.
21. Sommer, B., Kohler, M., Sprengel, R. and Seeburg, P.H. (1991) RNA editing in brain controls a determinant of ion flow in glutamate-gated channels. *Cell*, **67**, 11–19.
22. Kawahara, Y., Ito, K., Sun, H., Aizawa, H., Kanazawa, I. and Kwak, S. (2004) Glutamate receptors: RNA editing and death of motor neurons. *Nature*, **427**, 801.
23. Naciff, J.M., Behbehani, M.M., Misawa, H. and Dedman, J.R. (1999) Identification and transgenic analysis of a murine promoter that targets cholinergic neuron expression. *J. Neurochem.*, **72**, 17–28.
24. Tateno, M., Fukunishi, Y., Komatsu, S., Okazaki, Y., Kawai, J., Shibata, K., Itoh, M., Muramatsu, M., Held, W.A. and Hayashizaki, Y. (2001) Identification of a novel member of the snail/Gfi-1 repressor family, mlt 1, which is methylated and silenced in liver tumors of SV40 T antigen transgenic mice. *Cancer Res.*, **61**, 1144–1153.
25. Li, M., Ona, V.O., Guegan, C., Chen, M., Jackson-Lewis, V., Andrews, L.J., Olszewski, A.J., Stieg, P.E., Lee, J.P., Przedborski, S. *et al.* (2000) Functional role of caspase-1 and caspase-3 in an ALS transgenic mouse model. *Science*, **288**, 335–339.
26. Zhu, S., Stavrovskaya, I.G., Drozda, M., Kim, B.Y., Ona, V., Li, M., Sarang, S., Liu, A.S., Hartley, D.M., Wu du, C. *et al.* (2002) Minocycline inhibits cytochrome c release and delays progression of amyotrophic lateral sclerosis in mice. *Nature*, **417**, 74–78.
27. Drachman, D.B., Frank, K., Dykes-Hoberg, M., Teismann, P., Almer, G., Przedborski, S. and Rothstein, J.D. (2002) Cyclooxygenase 2 inhibition protects motor neurons and prolongs survival in a transgenic mouse model of ALS. *Ann. Neurol.*, **52**, 771–778.
28. van Gurp, M., Festjens, N., van Loo, G., Saelens, X. and Vandenabeele, P. (2003) Mitochondrial intermembrane proteins in cell death. *Biochem. Biophys. Res. Commun.*, **304**, 487–497.
29. Bezzi, P., Carmignoto, G., Pasti, L., Vesce, S., Rossi, D., Rizzini, B.L., Pozzan, T. and Volterra, A. (1998) Prostaglandins stimulate calcium-dependent glutamate release in astrocytes. *Nature*, **391**, 281–285.
30. Hall, E.D., Oostveen, J.A. and Gurney, M.E. (1998) Relationship of microglial and astrocytic activation to disease onset and progression in a transgenic model of familial ALS. *Glia*, **23**, 249–256.
31. Mattiazzi, M., D'Aurelio, M., Gajewski, C.D., Martushova, K., Kiaei, M., Beal, M.F. and Manfredi, G. (2002) Mutated human SOD1 causes dysfunction of oxidative phosphorylation in mitochondria of transgenic mice. *J. Biol. Chem.*, **277**, 29626–29633.
32. Okado-Matsumoto, A. and Fridovich, I. (2001) Subcellular distribution of superoxide dismutases (SOD) in rat liver: Cu,Zn-SOD in mitochondria. *J. Biol. Chem.*, **276**, 38388–38393.
33. Ookawara, T., Kawamura, N., Kitagawa, Y. and Taniguchi, N. (1992) Site-specific and random fragmentation of Cu,Zn-superoxide dismutase by glycation reaction. Implication of reactive oxygen species. *J. Biol. Chem.*, **267**, 18505–18510.
34. Urushitani, M., Kurisu, J., Tsukita, K. and Takahashi, R. (2002) Proteasomal inhibition by misfolded mutant superoxide dismutase 1 induces selective motor neuron death in familial amyotrophic lateral sclerosis. *J. Neurochem.*, **83**, 1030–1042.
35. Rakhit, R., Cunningham, P., Furtos-Matei, A., Dahan, S., Qi, X.F., Crow, J.P., Cashman, N.R., Kondejewski, L.H. and Chakrabartty, A. (2002) Oxidation-induced misfolding and aggregation of superoxide dismutase and its implications for amyotrophic lateral sclerosis. *J. Biol. Chem.*, **277**, 47551–47556.
36. Andrus, P.K., Fleck, T.J., Gurney, M.E. and Hall, E.D. (1998) Protein oxidative damage in a transgenic mouse model of familial amyotrophic lateral sclerosis. *J. Neurochem.*, **71**, 2041–2048.
37. Liu, R., Althaus, J.S., Ellerbrock, B.R., Becker, D.A. and Gurney, M.E. (1998) Enhanced oxygen radical production in a transgenic mouse model of familial amyotrophic lateral sclerosis. *Ann. Neurol.*, **44**, 763–770.
38. Liu, D., Wen, J., Liu, J. and Li, L. (1999) The roles of free radicals in amyotrophic lateral sclerosis: reactive oxygen species and elevated oxidation of protein, DNA, and membrane phospholipids. *FASEB J.*, **13**, 2318–2328.
39. Clement, A.M., Nguyen, M.D., Roberts, E.A., Garcia, M.L., Boillee, S., Rule, M., McMahon, A.P., Doucette, W., Siwek, D., Ferrante, R.J. *et al.* (2003) Wild-type nonneuronal cells extend survival of SOD1 mutant motor neurons in ALS mice. *Science*, **302**, 113–117.
40. Orrenius, S., McConkey, D.J., Bellomo, G. and Nicotera, P. (1989) Role of Ca^{2+} in toxic cell killing. *Trends Pharmacol. Sci.*, **10**, 281–285.
41. Alexianu, M.E., Ho, B.K., Mohamed, A.H., La Bella, V., Smith, R.G. and Appel, S.H. (1994) The role of calcium-binding proteins in selective motoneuron vulnerability in amyotrophic lateral sclerosis. *Ann. Neurol.*, **36**, 846–858.
42. Carriedo, S.G., Sensi, S.L., Yin, H.Z. and Weiss, J.H. (2000) AMPA exposures induce mitochondrial Ca(2+) overload and ROS generation in spinal motor neurons *in vitro*. *J. Neurosci.*, **20**, 240–250.
43. Rao, S.D., Yin, H.Z. and Weiss, J.H. (2003) Disruption of glial glutamate transport by reactive oxygen species produced in motor neurons. *J. Neurosci.*, **23**, 2627–2633.

44. Bendotti, C., Tortarolo, M., Suchak, S.K., Calvaresi, N., Carvelli, L., Bastone, A., Rizzi, M., Rattray, M. and Mennini, T. (2001) Transgenic SOD1 G93A mice develop reduced GLT-1 in spinal cord without alterations in cerebrospinal fluid glutamate levels. *J. Neurochem.*, **79**, 737–746.
45. Rao, S.D. and Weiss, J.H. (2004) Excitotoxic and oxidative cross-talk between motor neurons and glia in ALS pathogenesis. *Trends Neurosci.*, **27**, 17–23.
46. Suzuki, T., Miura, M., Nishimura, K. and Aosaki, T. (2001) Dopamine-dependent synaptic plasticity in the striatal cholinergic interneurons. *J. Neurosci.*, **21**, 6492–6501.
47. Inoue, H., Tsukita, K., Iwasato, T., Suzuki, Y., Tomioka, M., Tateno, M., Nagao, M., Kawata, A., Saido, T.C., Miura, M. *et al.* (2003) The crucial role of caspase-9 in the disease progression of a transgenic ALS mouse model. *EMBO J.*, **22**, 6665–6674.

THE JOURNAL OF BIOLOGICAL CHEMISTRY
© 2005 by The American Society for Biochemistry and Molecular Biology, Inc.

Vol. 280, No. 5, Issue of February 4, pp. 3390–3399, 2005
Printed in U.S.A.

Parkin Phosphorylation and Modulation of Its E3 Ubiquitin Ligase Activity*

Received for publication, July 9, 2004, and in revised form, November 12, 2004
Published, JBC Papers in Press, November 22, 2004, DOI 10.1074/jbc.M407724200

Ayako Yamamoto‡, Arno Friedlein§, Yuzuru Imai¶, Ryosuke Takahashi¶, Philipp J. Kahle‡‖, and Christian Haass‡

From the ‡Laboratory of Alzheimer's and Parkinson's Disease Research, Department of Metabolic Biochemistry, Ludwig Maximilians University, 80336 Munich, Germany, §Roche Center for Medical Genomics, F. Hoffmann-La Roche Ltd. 4070 Basel, Switzerland, and ¶Motor System Neurodegeneration, RIKEN Brain Science Institute, Saitama 351-0198, Japan

Mutations in the *PARKIN* gene are the most common cause of hereditary parkinsonism. The parkin protein comprises an N-terminal ubiquitin-like domain, a linker region containing caspase cleavage sites, a unique domain in the central portion, and a special zinc finger configuration termed RING-IBR-RING. Parkin has E3 ubiquitin-protein ligase activity and is believed to mediate proteasomal degradation of aggregation-prone proteins. Whereas the effects of mutations on the structure and function of parkin have been intensely studied, post-translational modifications of parkin and the regulation of its enzymatic activity are poorly understood. Here we report that parkin is phosphorylated both in human embryonic kidney HEK293 cells and human neuroblastoma SH-SY5Y cells. The turnover of parkin phosphorylation was rapid, because inhibition of phosphatases with okadaic acid was necessary to stabilize phosphoparkin. Phosphoamino acid analysis revealed that phosphorylation occurred mainly on serine residues under these conditions. At least five phosphorylation sites were identified, including Ser^{101}, Ser^{131}, and Ser^{136} (located in the linker region) as well as Ser^{296} and Ser^{378} (located in the RING-IBR-RING motif). Casein kinase-1, protein kinase A, and protein kinase C phosphorylated parkin *in vitro*, and inhibition of casein kinase-1 caused a dramatic reduction of parkin phosphorylation in cell lysates. Induction of protein folding stress in cells reduced parkin phosphorylation, and unphosphorylated parkin had slightly but significantly elevated autoubiquitination activity. Thus, complex regulation of the phosphorylation state of parkin may contribute to the unfolded protein response in stressed cells.

Parkinson's disease (PD)[1] is the second most common neurodegenerative disorder. Parkinsonian symptoms are caused by the progressive loss of dopaminergic neurons in the substantia nigra pars compacta (1). Although more than 90% of PD cases occur sporadically, the study of genetic mutations has offered great insight into the molecular mechanisms of PD (2). After the discovery that mutations in the *PARKIN* gene cause autosomal recessive juvenile parkinsonism (3), parkin mutations have been recognized as the most common cause of hereditary PD and possibly a risk factor for idiopathic PD (4, 5).

The *PARKIN* gene comprises 12 exons and codes for a 465-amino acid protein that is widely expressed, most prominently in muscle and throughout the brain (3). The 52-kDa parkin protein comprises an N-terminal ubiquitin-like domain (aa 1–76), a unique parkin domain (aa 145–232), and two RING (really interesting new gene) fingers (aa 238–293 and 418–449, respectively) flanking an IBR (in-between RING) domain (aa 314–377) at the C terminus. All of these domains appear to be functionally important, because PD mutations cluster in them (6).

Parkin functions in the ubiquitin-proteasome system as an E3 ubiquitin-protein ligase together with the E2 ubiquitin-conjugating co-enzymes UbcH7 or UbcH8 (7–9). Because this function appears to be defective in patients with parkin mutations, the identification of protein substrates is of great importance (6, 10). Parkin substrates include synaptic proteins (the septins CDCrel-1 and CDCrel-2, synaptotagmin XI, and the α-synuclein interactor synphilin-1), PaelR (parkin-associated endothelin-like receptor), cyclin E, α/β tubulin, and the p38 subunit of the aminoacyl-tRNA synthetase complex (9, 11–17). Parkin expression was found to be neuroprotective in *Drosophila* (18) and in cell culture models of dopamine neuron loss (19–22). However, the exact molecular mechanisms of how parkin dysfunction causes PD remain to be elucidated (6, 10).

Post-translational modifications often regulate enzymatic activity. Nitrosylation of parkin was recently found to occur in PD, leading to an inhibition of its ubiquitin ligase activity (23, 24). Here we addressed the question whether phosphorylation of parkin occurred and, if so, by which kinases under what cellular conditions. Parkin was found to be phosphorylated on at least five serine residues. Casein kinase-1 (CK-1), protein kinase A (PKA) and protein kinase C (PKC) were identified as parkin kinases *in vitro*, and inhibition of CK-1 suppressed phosphorylation of parkin in cell lysates. Unfolded protein stress mediated by proteasomal inhibition or endoplasmatic reticulum (ER) stress, but not oxidative stress, reduced the overall phosphorylation of parkin. Unphosphorylated parkin isolated from eukaryotic cells or purified as recombinant fusion protein from bacteria showed a small but significant increase of autoubiquitin ligase activity, compared with parkin phosphorylated *in vivo* and *in vitro*. Thus, we suggest that modulation of the phosphorylation state of parkin has a regulatory role on its E3 ubiquitin ligase activity.

* This work was supported by the German National Genome Research Network, the European Union (N)EUROPARK and APOPIS consortia and by Deutsche Forschungsgemeinschaft Grant SFB596. The costs of publication of this article were defrayed in part by the payment of page charges. This article must therefore be hereby marked "*advertisement*" in accordance with 18 U.S.C. Section 1734 solely to indicate this fact.

‖ To whom correspondence should be addressed. Tel.: 49-89-2180-75480; Fax: 49-89-2180-75415; E-mail: Philipp.Kahle@med.uni-muenchen.de.

[1] The abbreviations used are: PD, Parkinson's disease; aa, amino acid(s); CIP, calf intestinal alkaline phosphatase; CK, casein kinase; ER, endoplasmic reticulum; GST, glutathione *S*-transferase; MALDI, *matrix-assisted* laser desorption ionization; TOF, time-of-flight; OA, okadaic acid; PDBu, phorbol-12,13-dibutyrate; PKA, protein kinase A; PKC, protein kinase C; E1, ubiquitin-activating enzyme; E2, ubiquitin carrier protein; E3, ubiquitin-protein isopeptide ligase; PVDF, polyvinylidene difluoride; PKB, protein kinase B; ACTH, adrenocorticotropic hormone; RT, reverse transcription.

MATERIALS AND METHODS

Cell Culture, Transfection, and Establishment of Stable Transfectants—HEK293, HEK293T, and SH-SY5Y cells were cultured in Dulbecco's modified Eagle's medium with Glutamax (PAA Laboratories GmbH) supplemented with 10% fetal calf serum for HEK293 cells and HEK293T cells or 15% for SH-SY5Y cells. Cells were transfected using Lipofectamine 2000 Reagent (Invitrogen) or FuGene (Roche Applied Science) according to the supplier's instructions. Stable HEK293 and SH-SY5Y transfectants were selected with 200 or 22.5 μg/ml zeocin, respectively.

Construction of cDNAs—Human full-length parkin was amplified by PCR (all primer sequences are available upon request) using a parkin cDNA construct (a gift from R. Baumeister) and cloned into the XbaI/HindIII restriction sites of pcDNA3.1 zeo(−) (Invitrogen), yielding MYC-parkin.

An additional C-terminal V5 tag was introduced by subcloning into pcDNA6/V5-His (Invitrogen) (MYC-parkin-V5). For mapping the phosphorylation sites, parkin fragments comprising the N terminus (aa 2–144), the N terminus and middle portion (aa 2–293), and the C terminus (aa 294–465) were generated by PCR using the appropriate oligonucleotide primers and cloned into the XbaI/HindIII restriction sites of pcDNA3.1 zeo(−) or the NheI/EcoRI restriction enzyme sites of pcDNA6/V5-His, yielding the constructs MYC-parN(-V5), MYC-parNM(-V5), and MYC-parC(-V5). Serine-to-alanine mutants were generated by mutagenizing respective codons in MYC-parN-V5 or MYC-parC-V5 in two-step PCR.

GST-parkin, GST-parN, and GST-parC were constructed by PCR and cloned into the EcoRI/NotI restriction sites of pGEX-4T-1 (Amersham Biosciences). Serine-to-alanine mutants were generated by mutagenizing the respective codons in GST-parN or GST-parC by two-step PCR. N-terminal FLAG-tagged parkin (FLAG-parkin) and C-terminal FLAG-tagged PaeIR (PaeIR-FLAG) were described elsewhere (8, 11).

RT-PCR—Total RNA was isolated from both HEK293 cells and stable HEK293 transfectants of parkin under various stresses using peqGOLD RNA Pure (PeQLab). First strand cDNA was synthesized using SuperScript First-Strand Synthesis System for RT-PCR (Invitrogen). RT-PCR was performed using *Taq* DNA polymerase (PeQLab) and the following primers: BiP forward primer, 5′-CCGCATCACGCCGTC-3′; BiP reverse primer, 5′-GGCTCGTTGATGATCCTC-3′.

Immunoprecipitation and Immunoblotting—Cells were harvested 24 h after the transfection and lysed in lysis buffer (10 mM Tris-HCl, pH 7.5, 150 mM NaCl, 1 mM EDTA, and 1% Triton X-100) with proteinase inhibitors (Sigma) on ice for 15 min. Cell lysates were centrifuged at 4 °C at 16,000 × *g* for 20 min. Immunoprecipitations were carried out using protein G-Sepharose (Amersham Biosciences) or protein A-Sepharose, anti-Myc-agarose, anti-FLAG M2-agarose affinity gel (all from Sigma) at 4 °C for 2 h. Immunoprecipitates were washed with lysis buffer three times (or, in the case of radiolabeled samples, six times). Whole cell extracts and immunoprecipitates were separated by SDS-PAGE, and proteins were transferred onto PVDF membrane (Immobilon; Millipore Corp.). Enhanced chemiluminescence detection reagents (Amersham Biosciences) were used to detect immunoblot signals of the following antibodies: 9E10 monoclonal anti-Myc (Developmental Studies Hybridoma Bank, University of Iowa), monoclonal anti-V5 (Invitrogen), monoclonal anti-KDEL against glucose-regulated proteins Grp78 and Grp94 (Stressgen), polyclonal anti-parkin (Cell Signaling), and PRK8 monoclonal anti-parkin (25) (kindly provided by V. Lee).

In Vivo Phosphorylation Assay—Twenty-four h after the transfection, cells were incubated for 45 min in phosphate-free medium (Sigma), and 13–36 MBq of [^{32}P]orthophosphate was added. After 30 min (to label transfected parkin) or 2 h (to label endogenous parkin), 1 μM okadaic acid (OA) was added and incubated at 37 °C for 1 h. The conditioned medium was aspirated, and the cell monolayer washed twice with ice-cold phosphate-buffered saline. Cells were lysed on ice with lysis buffer, and immunoprecipitations were performed as above. Immunoprecipitates were separated by SDS-PAGE and transferred onto PVDF membrane. Autoradiography was carried out to visualize radiolabeled proteins.

Matrix-assisted Laser Desorption Ionization Time-of-flight (MALDI-TOF) Mass Spectrometry—Phosphorylation of transfected MYC-parkin fragments was induced with OA, and MYC immunoprecipitates were subjected to SDS-PAGE. Colloidal blue-stained bands of interest were in-gel digested with endoproteinase Lys-C as described (26). After overnight digestion, about 1 μl was mixed with 1 μl of saturated α-cyano-cinnamic acid in 50% acetonitrile, 0.1% trifluoroacetic acid in water and applied to the MALDI target. The samples were analyzed with a Bruker Daltonics (Bremen, Germany) Ultraflex TOF/TOF mass spectrometer.

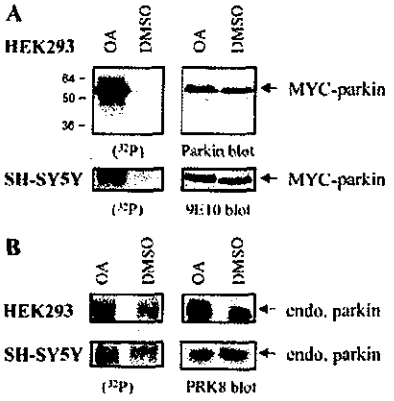

FIG. 1. **Parkin is phosphorylated both in HEK293 cells and SH-SY5Y cells.** *A*, HEK293 cells (*upper panels*) and SH-SY5Y cells (*lower panels*) stably expressing MYC-parkin were labeled with [^{32}P]orthophosphate in the presence or absence of OA, and then cell lysates were immunoprecipitated with 9E10. Proteins separated by 12% SDS-PAGE were transferred onto PVDF membrane. Autoradiography was carried out in order to visualize phosphorylated parkin (*left panels*). Afterward, blots were probed with polyclonal anti-parkin or 9E10 anti-Myc (*right panels*). *B*, endogenous parkin in HEK293 cells (*upper panels*) and SH-SY5Y cells (*lower panels*) was labeled with [^{32}P]orthophosphate and immunoprecipitated with polyclonal anti-parkin. After the autoradiography (*left panels*), blots were probed with PRK8 monoclonal anti-parkin (*right panels*). *DMSO*, Me_2SO.

An acceleration voltage of 25 kV was used. Calibration was internal to the samples with des-Arg-bradykinin and ACTH-(18–38) (both peptides purchased from Sigma).

Nanoelectrospray Ionization Tandem Mass Spectrometry—In order to identify which of the three possible serines was phosphorylated in the parkin peptide obtained after digestion with endoproteinase Lys-C with a monoisotopic mass of 1568.75 Da, this proteolytic product was subjected to nanoelectrospray ionization tandem mass spectrometry on a QSTAR Pulsar I quadrupole TOF tandem mass spectrometer (Applied Biosystems/MDS-Sciex, Toronto, Canada) equipped with a nanoelectrospray ion source (Proxeon, Odense, Denmark) as described (27).

Dephosphorylation by Alkaline Phosphatase—HEK293 cells and SH-SY5Y cells were transiently transfected with MYC-parkin-V5 and various portions of parkin (MYC-parN-V5, MYC-parNM-V5, and MYC-parC-V5). Twenty-four h after the transfection, 1 μM OA was added, and cells were incubated for 1 h. Immunoprecipitation using anti-Myc-agarose conjugate (Sigma) was performed. Immunoprecipitates were incubated at 37 °C for 1 h with or without calf intestinal alkaline phosphatase (CIP) (New England Biolabs) according to the supplier's manual. Reactions were terminated by adding 2× SDS sample buffer and analyzed by immunoblot.

Phosphoamino Acid Analysis—Phosphoamino acid analysis was performed using the method by Jelinek and Weber (28). After electroblotting radiolabeled proteins onto PVDF membrane, bands were excised and hydrolyzed using 6 N HCl at 100 °C for 90 min. After centrifugation, supernatants were dried in a SpeedVac concentrator. Pellets were dissolved in pH 2.5 buffer (5.9% glacial acetic acid, 0.8% formic acid, 0.3% pyridine, and 0.3 mM EDTA) and spotted onto thin layer chromatography plates (Merck) together with unlabeled phosphoamino acid markers (1 μg each of Ser(P), Thr(P), and Tyr(P); Sigma). One-dimensional high voltage electrophoresis was performed at 20 mA for 50 min. Radioactive phosphoamino acids were identified by autoradiography and co-migration with the ninhydrin-stained standards.

In Vitro Phosphorylation Assays—Recombinant rat CK-1 δ, recombinant α-subunit of human CK-2 and recombinant human Akt1/PKB protein kinase were used for *in vitro* phosphorylation assays according to the supplier's instructions (Cell Signaling). The catalytic subunit of PKA purified from bovine heart (gift from V. Kinzel) was used in a buffer containing 20 mM Tris, pH 7.5, 5 mM magnesium acetate, and 5 mM dithiothreitol. PKC purified from rat brain (Biomol) was used in a similar buffer to PKA supplemented with 1 μM phorbol-12,13-dibutyrate (PDBu), 0.5 mM $CaCl_2$, and 100 μg/ml phosphatidylserine under mixed micellar conditions. Fusion proteins GST-parkin, GST-parN, GST-parC, and various serine-to-alanine mutations in GST-parN or GST-parC were used as substrates. The reaction was started by adding 10 μM [γ-^{32}P]ATP (250 μM [γ-^{32}P]ATP in the case of Akt1/PKB) and allowed to proceed for 30 min at 30 °C.

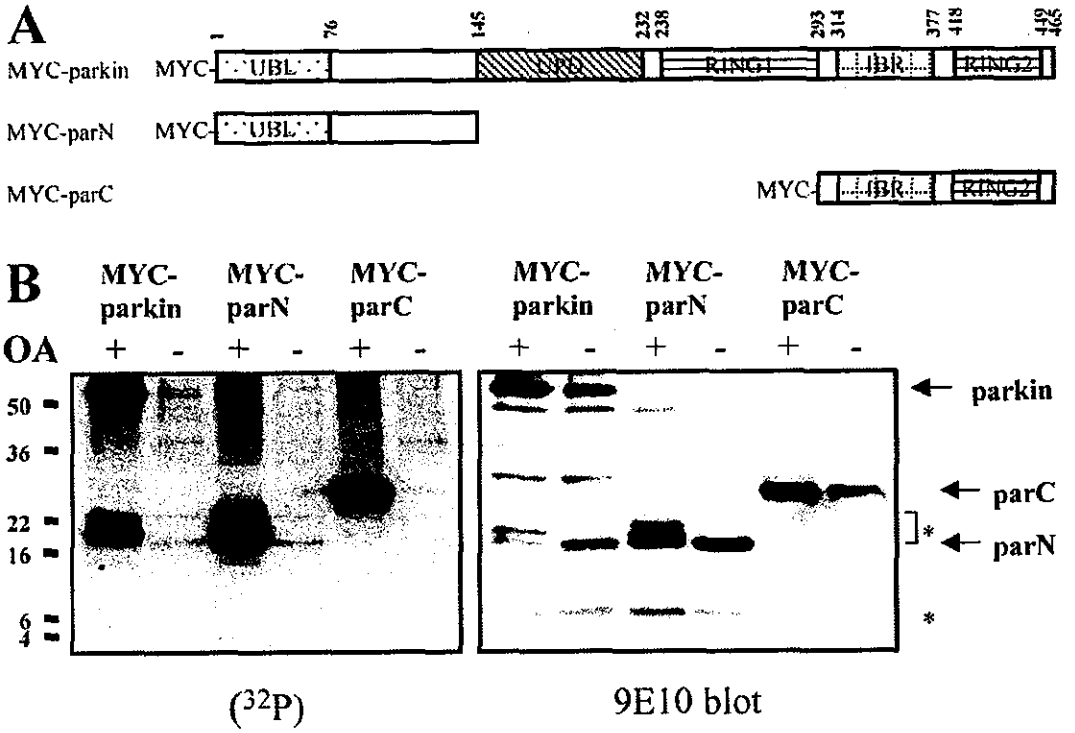

FIG. 2. **Both N terminus and C terminus of parkin are phosphorylated.** *A*, schematic representation of MYC-parkin, MYC-parN, and MYC-parC, which were used to establish stable transfectants in HEK293 cells. *B*, the experimental procedure was followed as described in Fig. 1*A*. Autoradiography was carried out in order to visualize phosphorylated parkin (*left panel*). Afterward, the immunoblot was probed with 9E10 anti-Myc (*right panel*). *, cleaved forms of MYC-parkin.

Alternatively, cell lysates were used to phosphorylate fusion proteins of GST carrying parkin, parN, and parC. HEK293 cells were lysed in a buffer containing 20 mM Tris, pH 7.5, 5 mM magnesium acetate, 5 mM dithiothreitol, and 0.5% Triton X-100. In case of PKC, 0.5 mM $CaCl_2$, 1 μM PDBu, and 100 μg/ml phosphatidylserine were added. After centrifugation at 14,000 × *g* at 4 °C for 10 min, GST-parkin, GST-parN, GST-parC, or various serine-to-alanine mutants were added to supernatants. Phosphorylation reactions were started by adding [γ-^{32}P]ATP and allowed to proceed at 30 °C for 30 min in the presence of 4 μM OA and in the presence or absence of 5 μM hymenialdisine (donated by L. Meijer), 5 μM H-89 (Biomol), or 5 μM GF 109203X (Biomol). After the reaction, precipitations with glutathione-Sepharose (Amersham Biosciences) were carried out at 4 °C for 2 h. Precipitates were washed four times with phosphate-buffered saline and eluted by 2× SDS sample buffer.

In Vitro Ubiquitination Assay—FLAG-parkin was transfected into HEK293T cells. Twenty-four h after the transfection, 1 μM OA was added to cells and incubated for 50 min. Cells were harvested and lysed in lysis buffer. Alternatively, GST-parkin immobilized on glutathione-Sepharose, which was phosphorylated by CK-1, PKA, or PKC was used. Immunoprecipitates using anti-FLAG M2-agarose (Sigma) or immobilized phosphorylated GST-parkin were washed three times with lysis buffer and once with ubiquitination buffer (50 mM Tris-HCl, pH 7.4, and 5 mM $MgCl_2$). One mM dithiothreitol, 2 mM ATP, 100 ng of E1 (AFFINITI), 2 μg of UbcH7 (AFFINITI or MBL) and 5 μg of ubiquitin biotinylated using the EZ-Link Sulfo-NHS biotinylation kit (Pierce) were added to the immunoprecipitates. The reactions were conducted at 30 °C for 90 min and terminated by adding 2× SDS sample buffer. Reaction mixtures were resolved by 10% SDS-PAGE, and immunoblot was carried out using anti-FLAG M2 monoclonal antibody (Sigma) or streptavidin-peroxidase polymer (Sigma). Autoubiquitination (biotinylated) of parkin was quantified by densitometric scanning of the streptavidin-peroxidase developed blots. Image analysis was done using NIH Image version 1.62 (available on the World Wide Web at rsb.info.nih.gov/nih-image).

RESULTS

Parkin Is Constitutively Phosphorylated at the N Terminus and the C Terminus—In order to examine whether or not parkin is phosphorylated, we carried out *in vivo* phosphorylation assays. Stable HEK293 and SH-SY5Y transfectants expressing MYC-parkin were labeled with [^{32}P]orthophosphate. Phosphorylation was stabilized with OA, which inhibits phosphoprotein phosphatase 1, 2A, and 2B. Analysis of Myc-immunoprecipitated parkin by autoradiography revealed that full-length MYC-parkin undergoes phosphorylation both in HEK293 cells and SH-SY5Y cells (Fig. 1*A*). OA treatment also increased the [^{32}P]orthophosphate incorporation into endogenous parkin present at low levels in HEK293 and SH-SY5Y cells (Fig. 1*B*).

To assess which portion of parkin is phosphorylated, we generated Myc-tagged N-terminal parkin (aa 2–144) (parN) and C-terminal parkin (aa 294–465) (parC) constructs (Fig. 2*A*) and established their stable transfectants. Stable transfectants from the middle portion of parkin (aa 145–293) could not be established, possibly due to folding difficulties of the polypeptide. Both N-terminal and C-terminal parkin fragments were phosphorylated (Fig. 2*B*). We also noted in the anti-Myc immunoprecipitates phosphorylated protein bands that were possibly cleavage products derived from full-length parkin (29–31) and resembled the parN fragments in terms of $^{32}PO_4$ incorporation and band shift. Retarded electrophoretic motility of the phosphorylated bands was evident for N-terminal parkin fragments, whereas such a mobility shift was not observed in parC (Fig. 2*B*). Thus, parkin is phosphorylated in both N terminus (with mobility shift) and C terminus (without mobility shift).

In order to further prove that parkin is phosphorylated and the observed electrophoretic motility shift of parN is caused by the covalent incorporation of phosphate, parkin immunoprecipitates were dephosphorylated with CIP. For this set of experiments, HEK293 and SH-SY5Y cells were transiently transfected with double-tagged MYC-parkin-V5, MYC-parN-V5, and MYC-parC-V5 (Fig. 3*A*). Transiently transfected cells were treated with OA and lysed, and the washed Myc-agarose immunoprecipitates were incubated with or without CIP. Then samples were subjected to 10–15% Tris/glycine gel electro-

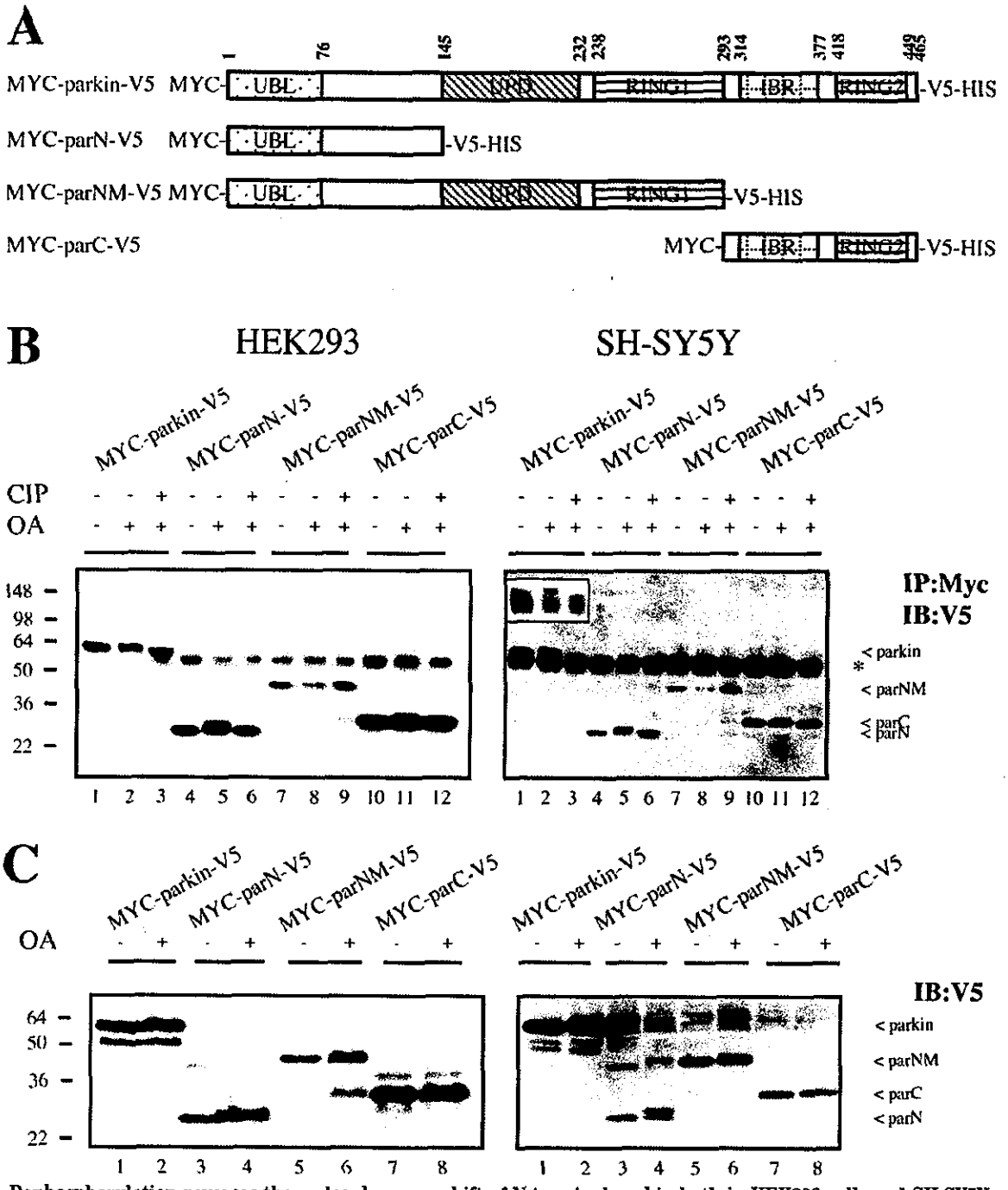

FIG. 3. **Dephosphorylation reverses the molecular mass shift of N-terminal parkin both in HEK293 cells and SH-SY5Y cells.** *A*, schematic representation of MYC-parkin-V5, MYC-parN-V5, MYC-parNM-V5, and MYC-parC-V5. *B*, the indicated constructs were transiently transfected into HEK293 cells (*left panels*) and SH-SY5Y cells (*right panels*). Twenty-four h after the transfection, 1 μM OA (*lanes 2, 3, 5, 6, 8, 9, 11,* and *12*) or Me_2SO (*lanes 1, 4, 7,* and *10*) was added and cultured for 2 h. Immunoprecipitation (*IP*) was carried out using MYC-agarose beads. Immunoprecipitates were incubated in the presence (*lanes 3, 6, 9,* and *12*) or absence (*lanes 1, 2, 4, 5, 7, 8, 10,* and *11*) of CIP. Samples were subjected to 10–20% Tris-glycine gel (Invitrogen) or 15% SDS-PAGE. *, unspecific band. The band shifts of full-length parkin from SH-SY5Y cells are better seen on a short exposure (*inset*). *C*, parkin expression levels in each transient transfectant treated with Me_2SO (*lanes 1, 3, 5,* and *7*) or OA (*lanes 2, 4, 6,* and *8*) were confirmed by immunoblotting (*IB*) of cell lysates using anti-V5 antibody (*lower panels*).

phoresis, and immunoblots were probed with anti-V5 antibody. MYC-parN-V5 immunoprecipitated from OA-treated cells showed retarded electrophoretic mobility compared with controls (Fig. 3*B*). Full-length MYC-parkin-V5 also showed slight band retardation after OA treatment. These phosphorylation-induced band shifts were observed both in HEK293 and SH-SY5Y cells, indicating similar phosphorylation patterns in non-neuronal neuronal cells. The phosphorylation-induced band retardations were reversed upon CIP treatment (Fig. 3*B*), confirming that phosphorylation in the N terminus of parkin occurs along with a characteristic band shift. Electrophoretic mobility shift caused by the incorporation of covalent phosphate is frequently observed in phosphorylated proteins (*e.g.* tau (32) and the C-terminal fragment of presenilin-1 (33)). On the other hand, band shifts were hardly observed in parNM and parC, despite the fact that parC was phosphorylated *in vivo* (Fig. 2). Note that a band shift is not always a consequence of phosphorylation (34).

Identification of Parkin Phosphorylation Sites—To identify the phosphorylated residues of parkin in OA-treated cells, phosphoamino acid analysis was carried out. Stable transfectants of MYC-parkin in HEK293 cells and SH-SY5Y cells as well as MYC-parN and MYC-parC in HEK293 cells were labeled with [^{32}P]orthophosphate in the presence of OA. Myc immunoprecipitates were subjected to SDS-PAGE and then transferred onto PVDF. Proteins were eluted from the excised bands and hydrolyzed. Phosphoamino acid analysis revealed that parkin was mainly phosphorylated at serine residues in OA-treated HEK293 cells and SH-SY5Y cells (Fig. 4). Some minor threonine phosphorylation was observed, whereas tyrosine phosphorylation was not evident under these conditions.

There are 30 serine residues in parkin, 14 of them in parN and 4 in parC. We carried out site-directed mutagenesis to identify phosphorylated serine sites. Selected serines with high phosphorylation probability identified with the NetPhos 2.0 prediction algorithm were substituted by alanine in order to generate unphosphorylatable forms. Since there are only 4 serines in parC (Ser^{296}, Ser^{378}, Ser^{384}, and Ser^{407}), we mutagenized all of them. These serine-to-alanine mutants in parN and parC as well as wild type with Myc tag at the N terminus and V5 tag at the C terminus were transiently transfected into HEK293 cells, and then cells were labeled with [^{32}P]orthophosphate in the presence or absence of OA. Cell lysates were subjected to immunoprecipitation using Myc-agarose beads. Phosphate incorporation of S101A, S131A, and S136A mutations under the treatment of OA were reduced compared with wild type parN (Fig. 5*A*). In the case of [S101A]parN, the shifted band was no longer detected. Thus, Ser^{101} was found to be the responsible phosphate acceptor for the motility shift of parN. $^{32}PO_4$ incorporation into the lower band was detectable but reduced for the S101A, S131A, and S136A mutants of parN. We also carried out mass spectrometry to determine phosphorylation sites in parN and confirmed that Ser^{131} and Ser^{136} (Fig. 5, *B* and *C*) were unambiguously phosphorylated, with weaker signals for Ser^{131} than for Ser^{136}. The phosphorylation of Ser^{101} was not detected by mass spectrometry analysis, since Lys-C proteolysis of parN could not provide complete coverage of the protein sequence.

In the case of parC, S296A was the only mutant that revealed a small but reproducible reduction of phosphate incorporation compared with wild type parC in the presence of OA (Fig. 5*D*). No difference of phosphate incorporation between wild type parC and mutants S384A and S407A was detected. However, Ser^{378} was clearly identified as phosphorylation site using an alternative assay (see below). Taken together, we discovered that Ser^{101}, Ser^{131}, and Ser^{136} in the parkin N terminus as well as Ser^{296} (Fig. 5) and Ser^{378} (see Fig. 7*B*) in the parkin C terminus are phosphorylated.

Parkin Is Phosphorylated by CK-1, PKA, and PKC—*In vitro* phosphorylation assays were carried out in order to identify kinases involved in phosphorylation of parkin. Fusion proteins GST-parkin, GST-parN, and GST-parC as well as mutations GST-[S101A]parN, GST-[S131A]parN, GST-[S136A]parN, GST-[S296A]parC, and GST-[S378A]parC were expressed in *Escherichia coli*. The recombinant parkin fusion proteins were incubated in the presence of [γ-^{32}P]ATP with various protein kinases. CK-1, CK-2, PKA, PKC were chosen because several recognition consensus sites for CK-2, PKA, and PKC were predicted by NetPhos 2.0 algorithm. The antiapoptotic kinase Akt/PKB1 was also considered, because parkin has been reported to protect dopaminergic cells against apoptosis (19–22). GST-parkin as well as GST-parN and GST-parC were efficiently phosphorylated by CK-1, PKA, and PKC, but not by CK-2 and Akt/PKB1 (Fig. 6*A*).

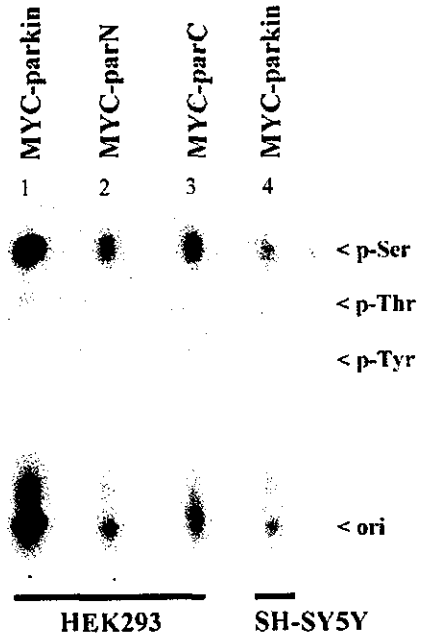

FIG. 4. **Parkin is phosphorylated mainly on serine residues.** HEK293 cells (*lanes 1–3*) and SH-SY5Y cells (*lane 4*) stably expressing the indicated MYC-parkin constructs were used for an *in vivo* phosphorylation assay labeled with [^{32}P]orthophosphate. Radiolabeled MYC-parkin (*lanes 1* and *4*), MYC-parN (*lane 2*), and MYC-parC (*lane 3*) were isolated by immunoprecipitation and subjected to one-dimensional phosphoamino acid analysis.

We analyzed further which kinases were responsible for selective phosphorylation of residues Ser^{101}, Ser^{131}, Ser^{136}, Ser^{296}, and Ser^{378}. *In vitro* phosphorylation assays were performed using GST fusion proteins harboring serine-to-alanine mutations. Phosphorylation by CK-1 was reduced in GST-[S101A]parN (Fig. 6*B*) and GST-[S378A]parC (Fig. 6*C*). We detected slightly reduced phosphorylation of GST-[S101A]parN, GST-[S131A]parN and GST-[S136A]parN by PKA, which indicates that PKA might possibly phosphorylate these serine sites. On the other hand, PKC-mediated phosphate incorporation was not reduced in the serine-to-alanine mutants investigated (Fig. 6, *B and C*). Thus, PKC was not responsible for phosphorylation of these sites.

We further analyzed whether CK-1, PKA and PKC phosphorylate GST-parN and GST-parC in cell lysates. Fusion proteins were incubated with extracts prepared from HEK293 cells, [γ-^{32}P]ATP, and OA in the presence or absence of selective inhibitor of CK-1 (hymenialdisine), an inhibitor of PKA (H-89), and an inhibitor of PKC (GF 109203X). PDBu was used to stimulate PKC activity. Consistent with the result from *in vitro* phosphorylation assays (Fig. 6), we found that GST-parN and GST-parC were phosphorylated by cellular extracts in the absence of inhibitors (Fig. 7, *A* and *B*). Both parN and parC phosphorylation was completely inhibited with the CK-1 inhibitor hymenialdisine (Fig. 7, *A* and *B*), but not in the presence of the PKA inhibitor H-89. Stimulation of PKC with PDBu enhanced phosphorylation of parN and parC, and this effect was reversed with the PKC inhibitor GF 109203X.

Consistent with the *in vitro* phosphorylation assays (Fig. 6), each of the serine-to-alanine mutants (S101A, S131A, S136A, S296A, and S378A) showed reduced phosphorylation in cell lysates (Fig. 7, *A* and *B*). The incorporation of phosphate was completely abolished when GST-[S378]parN was incubated with HEK293 lysates. Phosphate incorporation into the S296A mutant was also reduced in this assay, but to a lesser extent. Taken together, parkin is phosphorylated by CK-1, PKA, and

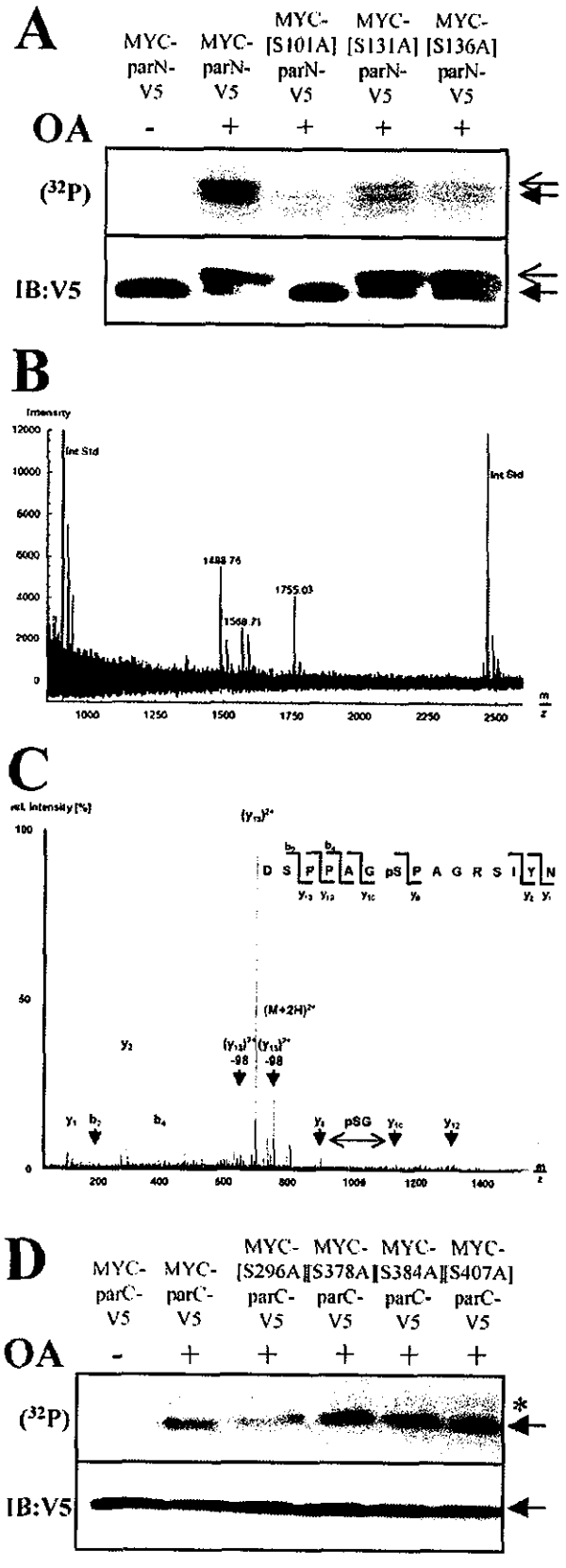

FIG. 5. **Parkin is phosphorylated at serines 101, 131, 136, and 296 in *in vivo* phosphorylation assays.** *A*, serines 101, 131, and 136 in MYC-parN-V5 were individually mutagenized to alanine. Each construct was transiently transfected into HEK293 cells and an *in vivo* phosphorylation assay was carried out with [^{32}P]orthophosphate in the presence or absence of OA. Cells were harvested, and immunoprecipitation using Myc-agarose beads was performed (*upper panels*). The *lower panels* reveal equal transfection efficiencies by immunoblotting (*IB*) using anti-V5 antibody. The *closed arrows* point to MYC-parN bands, and *open arrows* point to band-shifted, phosphorylated bands. *B*, MALDI-TOF mass spectrum of MYC-parN-V5 treated with OA after in-gel digest with endoproteinase Lys-C. The masses of the internal standards were as follows: MH^- – 2465.20-Da monoisotopic mass of ACTH-(18–39) and MH^- = 904.47-Da monoisotopic mass of des-Arg-bradykinin. Parkin-derived fragments were as follows: MH^+ = 1488.76-Da monoisotopic mass of unphosphorylated Lys-C peptide Asp^{130} to Asn^{144}, MH^+ = 1568.71-Da monoisotopic mass of phosphorylated Lys-C peptide Asp^{130} to Asn^{144}, and MH^+ = 1755.03-Da monoisotopic mass of Lys-C peptide Arg^{33} to Lys^{48}. *C*, the tandem mass spectrum of the doubly charged precursor ion (*m/z* 784.8) allowed the identification of the phosphorylation site within the peptide DSPPAGpSPAGRSIYN obtained after in-gel digestion with endoproteinase Lys-C. The phosphorylated amino acid and product ions derived from y ions by β-elimination of phosphoric acid are assigned. *D*, experimental procedures were carried out as described in *A*, except that serines 296, 378, 384, and 407 in MYC-parC-V5 were individually mutagenized to alanine.

PKC. CK-1 is a strong candidate kinase for phosphorylation of Ser^{101} in the parkin N terminus and Ser^{378} in the parkin C terminus (Fig. 7*C*).

Cellular Modulation of Parkin Phosphorylation—After having identified experimental conditions affecting parkin phosphorylation, we studied how cellular stress would influence parkin phosphorylation. Parkin has been shown to reduce oxidative stress (35) and protect against unfolded protein stress mediated by proteasome inhibitors (19) and ER stress (8, 11, 18). Thus, we have exposed HEK293 cells stably transfected with MYC-parkin-V5 to hydrogen peroxide, the proteasome inhibitor MG132, and the glycosylation inhibitor tunicamycin, concomitant with stabilization of phosphorylation by OA. As an alternative means to induce ER stress, cells were transfected with PaelR-FLAG, an aggregation-prone ER protein that mediates ER stress upon overexpression (11). Indeed, aggregation of PaelR-FLAG was readily detected on FLAG-probed Western blots (Fig. 8*A*).

ER stress was confirmed by determination of the co-regulated ER chaperones Grp78 and Grp94 (36, 37). Tunicamycin treatment caused induction of *GRP78* mRNA, as evidenced by RT-PCR, as well as Grp78 and Grp94 proteins, as evidenced by immunoblotting (Fig. 8*B*). PaelR overexpression caused an induction of these ER chaperones in HEK293 cells, an effect that was greatly reduced in parkin transfectants (Fig. 8*B*). Parkin expression also attenuated tunicamycin-induced glucose-regulated protein induction (Fig. 8*B*), consistent with previous reports that parkin protects cells against ER stress (8, 11).

[^{32}P]Orthophosphate incorporation into V5-immunoprecipitated MYC-parkin-V5 was found to be specifically reduced under conditions of protein folding stress. ER stress elicited by tunicamycin treatment and by PaelR overexpression greatly reduced overall parkin phosphorylation (Fig. 8). Proteasomal inhibition with MG-132 reduced parkin phosphorylation, but less than ER stress (Fig. 8). In contrast, oxidative stress mediated by hydrogen peroxide exposure did not affect parkin phosphorylation, although cytotoxicity became apparent after prolonged exposure to 60 μM H_2O_2. No ER stress was evidenced after H_2O_2 treatment (Fig. 8*B*). Thus, protein folding stress specifically reduces parkin phosphorylation.

OA-stabilized Phosphorylation of Parkin Suppresses E3 Activity—In order to examine whether phosphorylation can affect the enzymatic activity of parkin, *in vitro* ubiquitination assays were performed. Since it has been reported that parkin is autoubiquitinated (7–9), we used parkin itself as a substrate. For this purpose, HEK293T cells were transfected with FLAG-parkin as well as phosphoserine mutants. After OA or control treatment, cell lysates were prepared, and

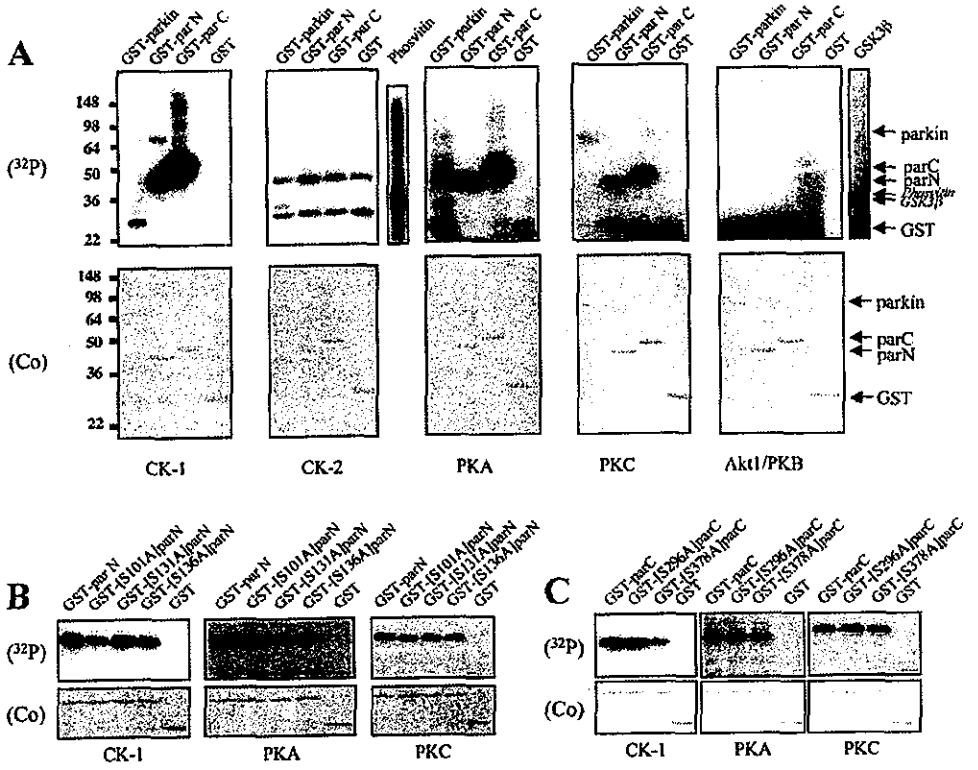

FIG. 6. **CK-1, PKA, and PKC phosphorylate parkin.** *A*, GST-parkin, GST-parN, and GST-parC were incubated with purified CK-1, CK-2, PKA, PKC, and Akt/PKB1 *in the presence of* [γ-^{32}P]ATP. Reaction mixtures were subjected to 12% SDS-PAGE. Phosphorylated fusion proteins were detected by autoradiography (*upper panels*). Phosvitin, histone, or GSK fusion protein was used as control substrate to confirm activity of CK-1/CK-2, PKA/PKC, or Akt/PKB1, respectively. Equal fusion protein loadings were shown by Coomassie staining (*lower panels*). *B* and *C*, *in vitro* phosphorylation assays were carried out with CK-1 (*left panels*) PKA (*middle panels*), and PKC (*right panels*) using the indicated GST-parN (*B*) or GST-parC (*C*) substrates. Experimental procedures were carried out as described in *A*. Equal substrate protein loading was confirmed by Coomassie staining (*lower panels*).

anti-FLAG immunoprecipitates were added for reconstitution of an *in vitro* ubiquitination assay. The formation of high molecular weight smears of biotin-ubiquitin in the FLAG immunoprecipitates revealed autoubiquitination of parkin. Overall phosphorylation upon OA treatment of wild-type parkin-transfected cells caused some reduction of parkin autoubiquitination (Fig. 9*A*).

To provide more quantitative measures of the effect of phosphorylation on parkin activity, we conducted autoubiquitination assays using recombinant GST-parkin phosphorylated *in vitro* with CK-1, PKA, and PKC. Parkin phosphorylation by these kinases reduced parkin activity (Fig. 9*B*). *In vitro* phosphorylation of GST-parkin decreased its autoubiquitination activity by 24 ± 8% (n = 4) in the case of CK-1, by 44 ± 5% (n = 3) in the case of PKA, and by 39 ± 12% (n = 3) in the case of PKC (Fig. 9*C*). Thus, phosphorylation of parkin appears to down-regulate its ubiquitin ligase activity.

In the attempt to identify individual regulatory phosphorylation sites within parkin, we investigated FLAG-tagged constructs of the phosphorylation site serine-to-alanine and -aspartate mutants identified above. None of the individual phosphorylation sites investigated appeared to exert a unique regulatory role, as evidenced from densitometric quantification of the autoubiquitinated parkin bands (results not shown). Thus, if parkin E3 activity is regulated by phosphorylation, it must arise from multiple sites.

DISCUSSION

Here we demonstrate that parkin is phosphorylated both in nonneuronal and neuronal cell lines. Parkin appears to be dephosphorylated rapidly under steady state conditions, because the phosphate incorporation was hardly observed without stabilization with OA. At least 5 serine residues were identified as phosphorylation sites. The kinases CK-1, PKA, and PKC were found to phosphorylate parkin. In cells exposed to the Parkinson's disease relevant protein folding stress (38), overall parkin phosphorylation decreased. Unphosphorylated parkin tended to be more active. These findings suggest that phosphorylation of parkin contributes to the regulation of its ubiquitin ligase activity upon unfolded protein stress.

Phosphoamino acid analysis revealed that serine sites are mainly phosphorylated in OA-treated cells. Threonine residues may also be phosphorylated in parkin, because a weak signal was clearly detected. Site-directed mutagenesis combined with *in vivo* and *in vitro* phosphorylation assays led to the identification of Ser^{101}, Ser^{131}, Ser^{136}, Ser^{296}, and Ser^{378} as phosphorylation sites in parkin. The corresponding serine-to-alanine mutants showed reduced, but not abolished incorporation of phosphate. Thus, multiple phosphorylation sites exist in parkin.

CK-1, PKA, and PKC were identified as putative parkin kinases. Specifically, CK-1 is one kinase to phosphorylate Ser^{101} and Ser^{378}, because mutations of these sites to alanine strongly reduced incorporation of phosphate. However, the possibility cannot be excluded that other kinases are involved in phosphorylation at these serine sites. CK-1 is an unexpected kinase to phosphorylate parkin because there is no CK-1 recognition consensus sequence ((D/E)*XX*(S/T)) in the amino acid sequence of parkin. CK-1 is ubiquitously expressed and involved in various important cellular processes, including signal transduction. We also observed a slightly reduced incorporation of phosphate by PKA in S101A, S131A, and S136A, which means that PKA may contribute to phosphorylation of these

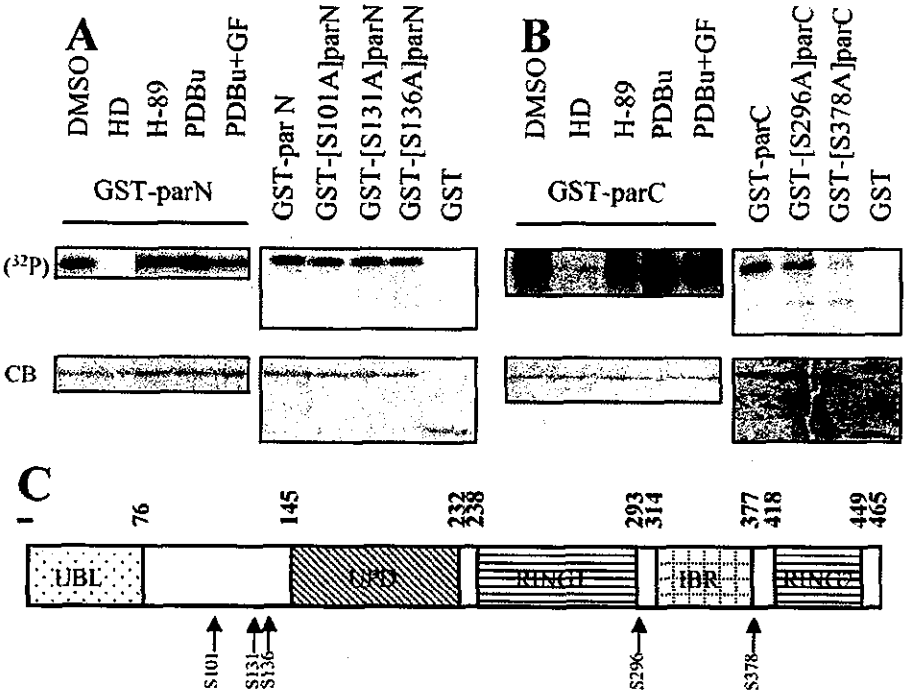

FIG. 7. **Phosphorylation of N terminus and C terminus by the extracts from HEK293 cells.** *A* and *B*, cellular extracts from HEK293 cells were incubated with GST-parN (*A*), GST-parC (*B*), and various serine-to-alanine mutants plus [γ-^{32}P]ATP and 4 μM OA in the presence or absence of CK-1-selective inhibitor hymenialdisine (5 μM), PKA-selective inhibitor H-89 (5 μM), and PKC-selective inhibitor GF 109203X (5 μM). In order to stimulate PKC, 1 μM PDBu was added. After the incubation, the precipitation using glutathione-Sepharose was carried out and subjected into 12% SDS-PAGE. Phosphorylated fusion proteins were detected by autoradiography (*upper panels*). Coomassie stain was carried out to prove the equal protein loading (*lower panels*). *C*, the *arrows* indicate phosphorylation sites in parkin. *DMSO*, Me_2SO.

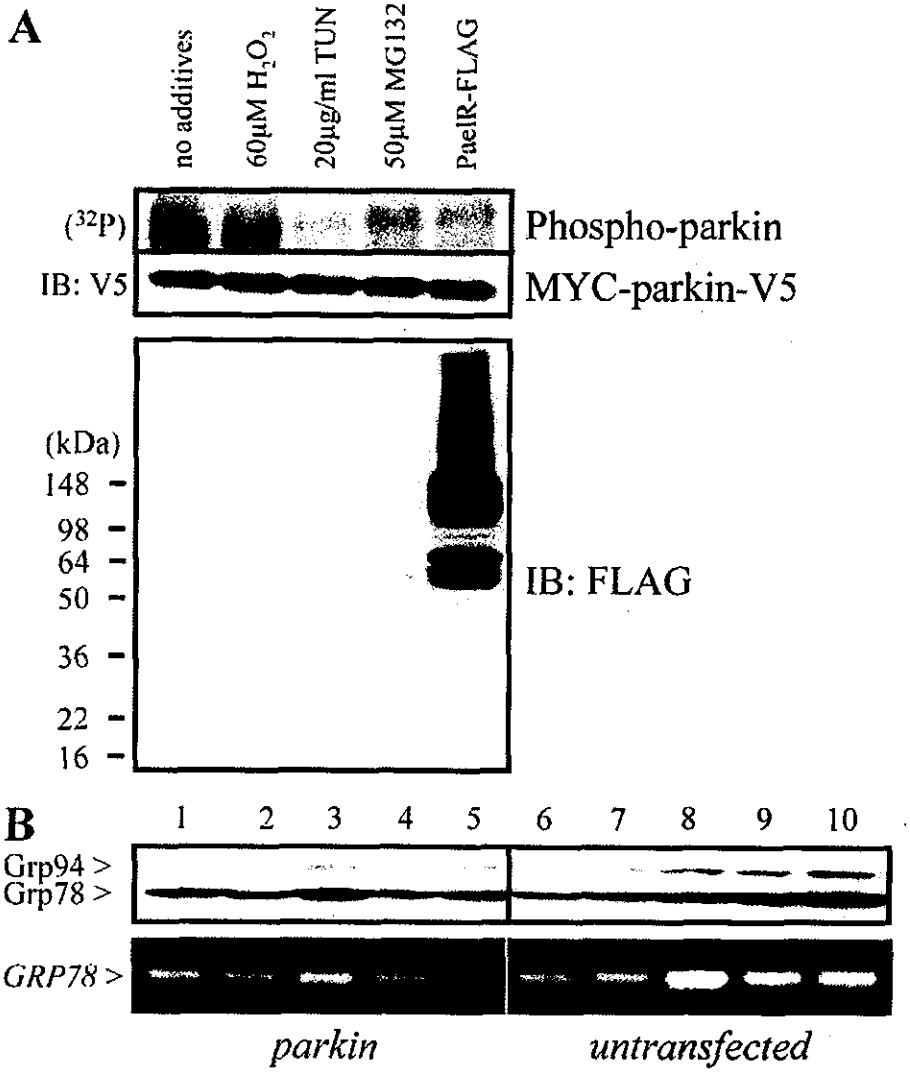

FIG. 8. **Phosphorylation of parkin is reduced by ER stress.** *A*, HEK293 cells stably expressing MYC-parkin-V5 were subjected to *in vivo* phosphorylation assay directly (*lanes 1–4*) or 24 h after transient transfection with PaeIR-FLAG (*lane 5*). During the $^{32}PO_4$ labeling, 1 μM OA (*lanes 1–5*) plus no additives (*lanes 1* and *5*), 60 μM H_2O_2 (*lane 2*), 20 μg/ml tunicamycin (*lane 3*), or 50 μM MG132 (*lane 4*) were administered. Anti-V5 immunoprecipitates were subjected to 12% SDS-PAGE. After electroblotting, phosphorylated proteins were detected by autoradiography (*upper panel*), and equal expression/loading was confirmed by probing with anti-V5 (*middle panel*). Overexpression and aggregation of PaeIR-FLAG was confirmed on parallel immunoblots (*IB*) probed with anti-FLAG (*lower panel*). *B*, ER stress was determined by immunoblotting of Grp78 and Grp94 protein (*upper panels*) and RT-PCR of *GRP78* mRNA (*lower panels*) in HEK293 cells stably transfected with MYC-parkin-V5 (*lanes 1–5*) or in untransfected HEK293 cells (*lanes 6–10*). All cells were treated for 3.5 h with 1 μM OA plus no additives (*lanes 1, 5, 6,* and *10*), 60 μM H_2O_2 (*lanes 2* and *7*), 20 μg/ml tunicamycin (*lanes 3* and *8*), or 50 μM MG132 (*lanes 4* and *9*).

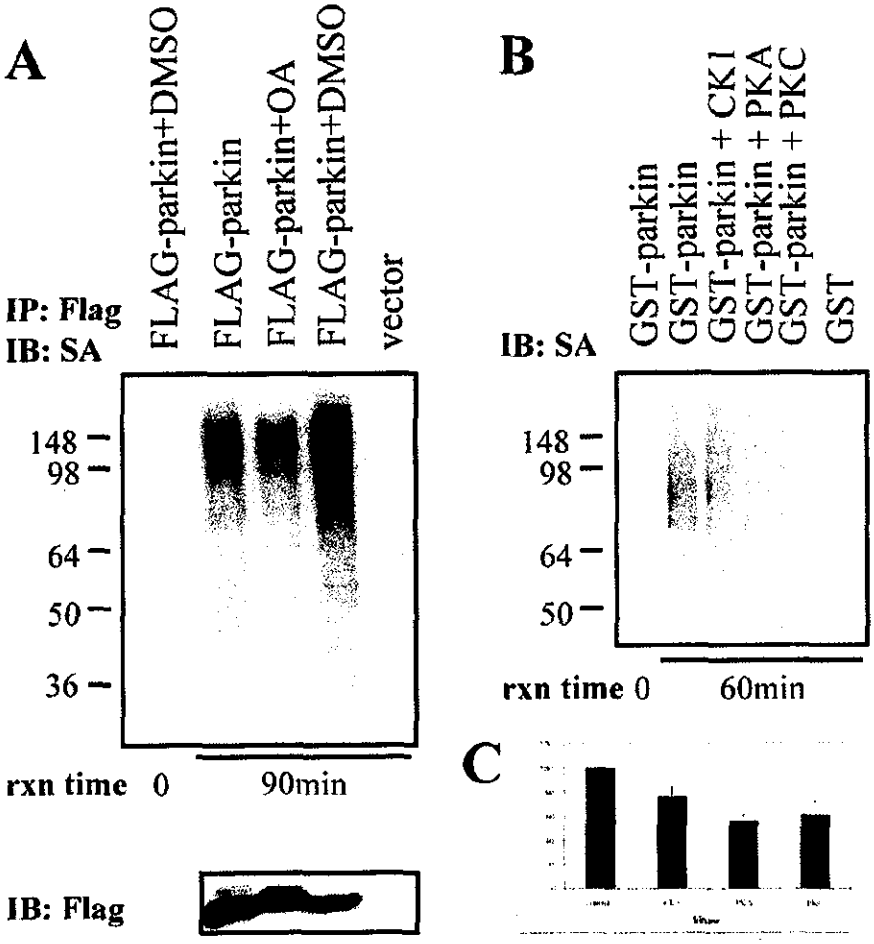

FIG. 9. **Phosphorylation down-regulates parkin autoubiquitination activity.** *A*, cellular extracts from transfected HEK293T cells in the presence or absence of OA and Me_2SO were subjected to immunoprecipitation (*IP*) using FLAG M2-agarose. Immunoprecipitates were incubated with E1, E2 (UbcH7), and biotin-ubiquitin at 30 °C for 90 min reaction (*rxn*) time (*upper panel*). Reaction mixtures were subjected to 10% SDS-PAGE and transferred onto PVDF membrane. Ubiquitinated parkin proteins were analyzed by immunoblot (*IB*) with streptavidin-peroxidase polymer (*upper panel*). Total lysates were analyzed by immunoblot with anti-FLAG antibody (*lower panel*). *B*, GST-parkin immobilized on glutathione-Sepharose was phosphorylated by CK-1, PKA, or PKC. The same experimental procedure was carried out as described in *A*. *C*, signal intensities of the streptavidin-binding biotinylated ubiquitin smears generated in experiments performed as described in *B* were quantified by densitometric scanning and expressed as a percentage of unphosphorylated parkin activity. *Error bars*, S.E. of four (CK-1) and three (PKA and PKC) experiments, respectively.

sites. PKC is able to phosphorylate parkin but is not responsible for the serine sites investigated here.

Since three identified phosphorylation sites were located in the linker region, and it has been reported that the ubiquitin-like domain interacts with Rpn10, a subunit of 19 S in proteasome (39), we also investigated whether parkin phosphorylation could affect proteasome activities. Each serine-to-alanine or -aspartate mutants still had almost the same level of activities as vector controls (data not shown). The RING-IBR-RING motif of parkin is important to interact with E2 co-enzymes. However, S296A and S378A did not consistently show reduced levels of ubiquitination by *in vitro* ubiquitination assays (data not shown). Although the RING-IBR-RING motif is crucial for parkin ubiquitin ligase function, single site phosphorylation in this domain appears to have no effect on autoubiquitination. Nevertheless, OA-mediated overall phosphorylation of parkin slightly reduced its E3 enzymatic activity. The regulation of parkin E3 activity must be due to multiple phosphorylation sites.

ER stress (but not oxidative stress) was found to specifically reduce parkin phosphorylation levels. Specifically, we found that OA-stabilized phosphorylation of parkin or phosphorylation by identified parkin kinases caused a small but significant reduction of parkin autoubiquitination activity. More *in vivo* work is needed to elucidate if and how parkin phosphorylation affects the activity and recognition of the various substrates of the E3 ubiquitin ligase parkin. In fact, some of the polyubiquitin signals detected in the *in vitro* E3 assay (Fig. 9) may arise from ubiquitination of co-purified, parkin-associated ubiquitin ligase substrates.

Because CK-1 appeared to be a major parkin kinase (Fig. 7), further investigations of signal transduction events involving CK-1 might be particularly revealing for the regulation of parkin E3 ubiquitin ligase activity. More generally, the involvement of parkin phosphorylation in the ER unfolded protein stress response (Fig. 8) might contribute to the understanding of parkin as dopaminergic neuron survival factor.

Taken together, we suggest that the reduced phosphorylation of parkin in ER stressed cells contributes to the up-regulation of parkin E3 ubiquitin ligase activity, which is believed to suppress cytotoxicity due to unfolded protein stress.

Acknowledgments—We thank J. Walter for technical advice, L. Meijer for providing hymenialdisine, V. Kinzel for the gift of PKA, and V. Lee for the donation of monoclonal anti-parkin. We are grateful to W. Springer, U. Leimer, R. Baumeister, and N. Hattory for parkin constructs.

REFERENCES

1. Dauer, W., and Przedborski, S. (2003) *Neuron* **39,** 889–909
2. Dawson, T. M., and Dawson, V. L. (2003) *Science* **302,** 819–822
3. Kitada, T., Asakawa, S., Hattori, N., Matsumine, H., Yamamura, Y., Minoshima, S., Yokochi, M., Mizuno, Y., and Shimizu, N. (1998) *Nature* **392,** 605–608
4. Lücking, C. B., Dürr, A., Bonifati, V., Vaughan, J., De Michele, G., Gasser, T., Harhangi, B. S., Meco, G., Denèfle, P., Wood, N. W., Agid, Y., and Brice, A. (2000) *N. Engl. J. Med.* **342,** 1560–1567
5. West, A., Periquet, M., Lincoln, S., Lücking, C. B., Nicholl, D., Bonifati, V., Rawal, N., Gasser, T., Lohmann, E., Deleuze, J.-F., Maraganore, D., Levey, A., Wood, N., Dürr, A., Hardy, J., Brice, A., and Farrer, M. (2002) *Am. J. Med. Genet.* **114,** 584–591
6. Kahle, P. J., and Haass, C. (2004) *EMBO Rep.* **5,** 681–685
7. Shimura, H., Hattori, N., Kubo, S., Mizuno, Y., Asakawa, S., Minoshima, S., Shimizu, N., Iwai, K., Chiba, T., Tanaka, K., and Suzuki, T. (2000) *Nat. Genet.* **25,** 302–305
8. Imai, Y., Soda, M., and Takahashi, R. (2000) *J. Biol. Chem.* **275,** *35661–35664*
9. Zhang, Y., Gao, J., Chung, K. K. K., Huang, H., Dawson, V. L., and Dawson, T. M. (2000) *Proc. Natl. Acad. Sci. U. S. A.* **97,** 13354–13359
10. Cookson, M. R. (2003) *Neuromolecular Med.* **3,** 1–13
11. Imai, Y., Soda, M., Inoue, H., Hattori, N., Mizuno, Y., and Takahashi, R. (2001)

Cell **105,** 891–902
12. Chung, K. K. K., Zhang, Y., Lim, K. L., Tanaka, Y., Huang, H., Gao, J., Ross, C. A., Dawson, V. L., and Dawson, T. M. (2001) *Nat. Med.* **7,** 1144–1150
13. Staropoli, J. F., McDermott, C., Martinat, C., Schulman, B., Demireva, E., and Abeliovich, A. (2003) *Neuron* **37,** 735–749
14. Ren, Y., Zhao, J., and Feng, J. (2003) *J. Neurosci.* **23,** 3316–3324
15. Corti, O., Hampe, C., Koutnikova, H., Darios, F., Jacquier, S., Prigent, A., Robinson, J.-C., Pradier, L., Ruberg, M., Mirande, M., Hirsch, E., Rooney, T., Fournier, A., and Brice, A. (2003) *Hum. Mol. Genet.* **12,** 1427–1437
16. Choi, P., Snyder, H., Petrucelli, L., Theisler, C., Chong, M., Zhang, Y., Lim, K., Chung, K. K. K., Kehoe, K., D'Adamio, L., Lee, J. M., Cochran, E., Bowser, R., Dawson, T. M., and Wolozin, B. (2003) *Mol. Brain Res.* **117,** 179–189
17. Huynh, D. P., Scoles, D. R., Nguyen, D., and Pulst, S. M. (2003) *Hum. Mol. Genet.* **12,** 2587–2597
18. Yang, Y., Nishimura, I., Imai, Y., Takahashi, R., and Lu, B. (2003) *Neuron* **37,** 911–924
19. Petrucelli, L., O'Farrell, C., Lockhart, P. J., Baptista, M., Kehoe, K., Vink, L., Choi, P., Wolozin, B., Farrer, M., Hardy, J., and Cookson, M. R. (2002) *Neuron* **36,** 1007–1019
20. Darios, F., Corti, O., Lücking, C. B., Hampe, C., Muriel, M. P., Abbas, N., Gu, W. J., Hirsch, E. C., Rooney, T., Ruberg, M., and Brice, A. (2003) *Hum. Mol. Genet.* **12,** 517–526
21. Higashi, Y., Asanuma, M., Miyazaki, I., Hattori, N., Mizuno, Y., and Ogawa, N. (2004) *J. Neurochem.* **89,** 1490–1497
22. Jiang, H., Ren, Y., Zhao, J., and Feng, J. (2004) *Hum. Mol. Genet.* **13,** 1745–1754
23. Chung, K. K. K., Thomas, B., Li, X., Pletnikova, O., Troncoso, J. C., Marsh, L., Dawson, V. L., and Dawson, T. M. (2004) *Science* **304,** 1328–1331
24. Yao, D., Gu, Z., Nakamura, T., Shi, Z.-Q., Ma, Y., Gaston, B., Palmer, L. A., Rockenstein, E. M., Zhang, Z., Masliah, E., Uehara, T., and Lipton, S. A. (2004) *Proc. Natl. Acad. Sci. U. S. A.* **101,** 10810–10814
25. Pawlyk, A. C., Giasson, B. I., Sampathu, D. M., Perez, F. A., Lim, K. L., Dawson, V. L., Dawson, T. M., Palmiter, R. D., Trojanowski, J. Q., and Lee, V. M.-Y. (2003) *J. Biol. Chem.* **278,** 48120–48128
26. Fountoulakis, M., and Langen, H. (1997) *Anal. Biochem.* **250,** 153–156
27. Wilm, M., and Mann, M. (1996) *Anal. Chem.* **68,** 1–8
28. Jelinek, T., and Weber, M. J. (1993) *BioTechniques* **15,** 628–630
29. Schlossmacher, M. G., Frosch, M. P., Gai, W. P., Medina, M., Sharma, N., Forno, L., Ochiishi, T., Shimura, H., Sharon, R., Hattori, N., Langston, J. W., Mizuno, Y., Hyman, B. T., Selkoe, D. J., and Kosik, K. S. (2002) *Am. J. Pathol.* **160,** 1655–1667
30. Kahns, S., Lykkebo, S., Jakobsen, L. D., Nielsen, M. S., and Jensen, P. H. (2002) *J. Biol. Chem.* **277,** 15303–15308
31. Kahns, S., Kalai, M., Jakobsen, L. D., Clark, B. F. C., Vandenabeele, P., and Jensen, P. H. (2003) *J. Biol. Chem.* **278,** 23376–23380
32. Lindwall, G., and Cole, R. D. (1984) *J. Biol. Chem.* **259,** 5301–5305
33. Walter, J., Grünberg, J., Capell, A., Pesold, B., Schindzielorz, A., Citron, M., Mendla, K., St George-Hyslop, P., Multhaup, G., Selkoe, D. J., and Haass, C. (1997) *Proc. Natl. Acad. Sci. U. S. A.* **94,** 5349–5354
34. Okochi, M., Walter, J., Koyama, A., Nakajo, S., Baba, M., Iwatsubo, T., Meijer, L., Kahle, P. J., and Haass, C. (2000) *J. Biol. Chem.* **275,** 390–397
35. Hyun, D.-H., Lee, M., Hattori, N., Kubo, S.-I., Mizuno, Y., Halliwell, B., and Jenner, P. (2002) *J. Biol. Chem.* **277,** 28572–28577
36. Munro, S., and Pelham, H. R. (1986) *Cell* **46,** 291–300
37. Chang, S. C., Erwin, A. E., and Lee, A. S. (1989) *Mol. Cell. Biol.* **9,** 2153–2162
38. Giasson, B. I., and Lee, V. M.-Y. (2001) *Neuron* **31,** 885–888
39. Sakata, E., Yamaguchi, Y., Kurimoto, E., Kikuchi, J., Yokoyama, S., Yamada, S., Kawahara, H., Yokosawa, H., Hattori, N., Mizuno, Y., Tanaka, K., and Kato, K. (2003) *EMBO Rep.* **4,** 301–306

Journal of Neurochemistry, 2004, **91**, 299–307 doi:10.1111/j.1471-4159.2004.02713.x

U-box protein carboxyl terminus of Hsc70-interacting protein (CHIP) mediates poly-ubiquitylation preferentially on four-repeat Tau and is involved in neurodegeneration of tauopathy

Shigetsugu Hatakeyama,*,‡ Masaki Matsumoto,*,‡ Takumi Kamura,*,‡ Miyuki Murayama,¶ Du-Hua Chui,¶ Emmanuel Planel,¶ Ryosuke Takahashi,§ Keiichi I. Nakayama*,†,‡ and Akihiko Takashima¶

**Department of Molecular and Cellular Biology and †Department of Molecular Genetics, Medical Institute of Bioregulation, Fukuoka, Japan*

‡CREST, Japan Science and Technology Corporation, Saitama, Japan

§Laboratory for Motor System Neurodegeneration and ¶Laboratory for Alzheimer's Disease, Brain Science Institute, RIKEN, Saitama, Japan

Abstract

Neurofibrillary tangles (NFTs), which are composed of hyperphosphorylated and ubiquitylated tau, are exhibited at regions where neuronal loss occurs in neurodegenerative diseases; however, the mechanisms of NFT formation remain unknown. Molecular studies of frontotemporal dementia with parkinsonism-17 demonstrated that increasing the ratio of tau with exon 10 insertion induced fibrillar tau accumulation. Here, we show that carboxyl terminus of Hsc70-interacting protein (CHIP), a U-box protein, recognizes the microtubule-binding repeat region of tau and preferentially ubiquitylates four-repeat tau compared with three-repeat tau. Overexpression of CHIP induced the prompt degradation of tau, reduced the formation of detergent-insoluble tau and inhibited proteasome inhibitor-induced cell death. NFT bearing neurons in progressive supranuclear palsy, in which four-repeat tau is a component, showed the accumulation of CHIP. Thus, CHIP is a ubiquitin ligase for four-repeat tau and maintains neuronal survival by regulating the quality control of tau in neurons.

Keywords: carboxyl terminus of Hsc70-interacting protein, neurodegeneration, neurofibrillary tangle, tau, ubiquitylation.

J. Neurochem. (2004) **91**, 299–307.

Protein aggregation causes the pathological lesions associated with neurodegenerative disorders (Kopito and Ron 2000). Neurofibrillary tangles (NFTs) emerge when pathological tau protein aggregates accumulate in neurons and form paired helical filament-tau proteins. These aggregates are composed of both ubiquitylated and highly phosphorylated tau and are characteristic of several neurodegenerative diseases, including Alzheimer's disease (Selkoe 2000; Lee *et al.* 2001; Hardy and Selkoe 2002). Of the several kinases that play a role in the hyperphosphorylation of paired helical filament-tau (Ishiguro *et al.* 1993; Morishima-Kawashima *et al.* 1995; Goedert *et al.* 1997), GSK-3β and JNK hyperphosphorylation leads to the formation of paired helical filament-like, detergent-insoluble tau (Sato *et al.* 2002). Tau gene mutations have recently been reported to cause frontotemporal dementia with parkinsonism-17, which has been characterized as exhibiting NFTs and neuron loss without β-amyloid peptide deposition in autopsied human brains, demonstrating that tau abnormalities alone can cause NFTs and neuronal death. While exonic mutations, such as P301L, affect the biochemical nature of tau and promote the self-assembly of mutant tau into filaments, intronic mutations within exon 10 or its 5′ splice regulatory region alter the ratio

Received January 19, 2004; revised manuscript received May 27, 2004; accepted June 11, 2004.

Address correspondence and reprint requests to Akihiko Takashima, Laboratory for Alzheimer's Disease, Brain Science Institute, RIKEN, Saitama 351-0198, Japan. E-mail: kenneth@brain.riken.jp

Abbreviations used: AD, Alzheimer's disease; CHIP, carboxyl terminus of Hsc70-interacting protein; EGFP, enhanced green fluorescent protein; GFP, green fluorescent protein; GST, glutathione S-transferase; HA, haemaglutinin; IB, immunoblot; IP, immunoprecipitate; NFT, neurofibrillary tangle; RNAi, RNA interference; SDS, sodium dodecyl sulfate; TPR, tetratricopeptide repeat; WCE, whole cell lysate.

of tau isoforms. In general, these mutations affect exon 10 splicing patterns thus altering the relative proportions of four- and three-repeat tau that are expressed. An increase in four-repeat tau induces the accumulation of four-repeat tau and NFT formation. We assumed that an impairment in a mechanism for four-repeat tau degradation would lead to four-repeat tau accumulation. As tau in NFTs is ubiquitylated, the ubiquitin proteasome may be the mechanism responsible for tau degradation in neurodegeneration (Mori *et al.* 1987) and the deterioration of this system might contribute to NFT formation. However, the mechanism by which the ubiquitylation of tau occurs is still unknown.

Protein ubiquitylation is mediated by a multienzyme cascade involving at least three distinct types of enzymes, a ubiquitin-activating enzyme (E1), a ubiquitin-conjugating enzyme (E2) and a ubiquitin-protein ligase (E3) (Hershko 1983). E3 enzymes catalyse the final step for substrate recognition in the ubiquitylation pathway. Currently there are two known E3 ligases, the HECT family E3s and adaptor E3s containing a RING finger or a U-box (Weissman 2001; Hatakeyama and Nakayama 2003). The carboxyl terminus of Hsc70-interacting protein (CHIP) has a U-box domain and was originally identified as a tetratricopeptide repeat (TPR)-containing protein that interacts with mammalian heat shock protein Hsc/Hsp70 (Ballinger *et al.* 1999). CHIP binds directly to the molecular chaperones Hsp90 or Hsc70 via TPR domains; therefore, when unfolded or misfolded proteins accumulate, CHIP may contribute to the cellular response. The combination of CHIP and Hsp90 mediates the ubiquitylation of the glucocorticoid receptor and CHIP with Hsc70 targets the immature cystic fibrosis transmembrane conductance regulator for proteasomal degradation (Connell *et al.* 2001; Meacham *et al.* 2001). We recently showed that the level of Hsp90 is reduced in tau-accumulated neurons of Tg mice expressing frontotemporal dementia with parkinsonism-17 tau mutations (Tanemura *et al.* 2001, 2002; Tatebayashi *et al.* 2002; Dou *et al.* 2003). This prompted us to investigate the possible involvement of CHIP in the poly-ubiquitylation of tau.

Materials and methods

Cell culture

HEK293T, COS7 or Neuro2A cells were cultured under an atmosphere of 5% CO_2 at 37°C in Dulbecco's modified Eagle's medium (Invitrogen; Carlsbad, CA, USA) supplemented with 10% fetal bovine serum (Invitrogen).

Cloning cDNAs and plasmid construction

The expression plasmids containing FLAG- or Myc-tagged mouse CHIP, mutants of these cDNAs [UFD2a, UFD2b, PRP19, IκBα, IKK2, haemaglutinin (HA)-tagged ubiquitin and wild type (four- and three-repeat)] and tau mutants were generated as previously described (Hatakeyama *et al.* 2001). To generate the mutant (P301L) of tau or Hsc70, we performed site-directed mutagenesis with a Quick Change kit (Stratagene, La Jolla, CA, USA) and with mutated oligonucleotide primers corresponding to each site.

Production of recombinant proteins in bacteria

Glutathione S-transferase (GST) fusion proteins were expressed in *Escherichia coli* strain DH5α cultured in the presence of 0.1 mM isopropyl-β-D-thiogalactopyranoside. Bacterial cells were resuspended in phosphate-buffered saline and lysed by sonication; cellular debris was removed by centrifugation for 20 min at 13 000 *g*. Glutathione-Sepharose 4B beads (Amersham Biosciences, Piscataway, NJ, USA) were added to the resulting supernatant fluid and the mixture was rotated at 4°C overnight. The beads were washed in phosphate-buffered saline and GST fusion proteins were eluted with 50 mM Tris-HCl (pH 8.0) containing 10 mM reduced glutathione.

Transfection, immunoprecipitation and immunoblot analysis

Cells were transfected using the calcium phosphate method and lysed in a lysis buffer containing 50 mM Tris-HCl (pH 7.4), 150 mM NaCl, 1% nonidet P-40, leupeptin (10 μg/mL), 1 mM phenylmethylsulfonyl fluoride, 400 μM Na_3VO_4, 400 μM EDTA, 1 mM EGTA, 10 mM NaF and 10 mM sodium pyrophosphate. The lysate was centrifuged at 16 000 *g* for 10 min at 4°C and the resulting supernatant fluid was incubated with antibodies for 2 h at 4°C. Protein G-Sepharose equilibrated in the same buffer was added to the mixture, which was then rotated for 1 h at 4°C. The resin was separated by centrifugation, washed four times with lysis buffer and then boiled in sodium dodecyl sulfate (SDS) sample buffer. Immunoblot analysis was performed with the following primary antibodies: anti-Myc (1 μg/mL; 9E10, Covance Inc., Princeton, NJ, USA), anti-FLAG (1 μg/mL; M5, Sigma-Aldrich, St. Louis, MO, USA), anti-HA (1 μg/mL; HA.11/16B12, Babco, Berkeley, CA, USA), anti-Hsp90 (1 μg/mL; 68, Transduction Laboratories, San Jose, CA, USA), anti-Hsp70 (1 μg/mL; 7, Transduction Laboratories), anti-CHIP (1 μg/mL, Hatakeyama and Nakayama 2003), $p27^{Kip1}$ (1 μg/mL; 57, Transduction Laboratories) and anti-ubiquitin (1 μg/mL; 1B3, MBL International, Woburn, MA, USA). Immune complexes were detected with horseradish peroxidase-conjugated antibodies to mouse or rabbit immunoglobulin G (1 : 10 000 dilution; Promega Corporation, Madison, WI, USA) and an enhanced chemiluminescence system (ECL; Amersham Biosciences).

Isolation of insoluble tau from cell lines

Cells were lysed with ristocetin-induced platelet agglutination buffer containing 1% SDS. Cell lysate (2 mg) was centrifuged for 20 min at 100 000 *g* at 4°C. The resulting pellet was washed four times with 300 μL of ristocetin-induced platelet agglutination buffer using a sonic homogenizer. The insoluble pellet was solubilized in 70% formic acid for use in the immunoblot analysis or resuspended in 100 mM Tris-HCl (pH 8.3) for examination using electron microscopy. Following centrifugation for 20 min at 100 000 *g* at 4°C, the formic acid fraction was collected, air-dried and subjected to immunoblot analysis after suspension in SDS gel loading buffer. The samples were resolved on SDS–polyacrylamide gel electrophoresis and immunoblot analysis was performed.

In vitro ubiquitylation assay

The *in vitro* ubiquitylation assay was performed as described previously (Hatakeyama *et al.* 2001). In brief, reaction mixtures (20 μL) containing 1 μg of recombinant GST-CHIP, 0.1 μg of recombinant rabbit E1 (Boston Biomedica, Boston, MA, USA), 1 μL of recombinant human Ubc4, 0.5 U of phosphocreatine kinase, 1 μg of GST-Ub (MBL), 25 mM Tris-HCl (pH 7.5), 120 mM NaCl, 2 mM ATP, 1 mM $MgCl_2$, 0.3 mM dithiothreitol and 1 mM creatine phosphate were incubated for 2 h at 30°C. The reaction was terminated by the addition of SDS sample buffer containing 4% 2ME and heating at 95°C for 5 min. Samples were resolved by SDS–polyacrylamide gel electrophoresis on a 6% gel and then subjected to immunoblot analysis with a mouse monoclonal antibody to tau (clone 15; Transduction Laboratories) and horseradish peroxidase-conjugated rabbit polyclonal antibody to mouse Ig (Promega). Signals were detected with ECL (Amersham Pharmacia).

Pulse-chase analysis with cycloheximide

Cells were cultured with cycloheximide at a concentration of 50 μg/mL and then incubated for various times. Cell lysates were then subjected to SDS–polyacrylamide gel electrophoresis and immunoblot analysis with antibody to Myc, Hsp90, FLAG and $p27^{Kip1}$.

RNA interference and retroviral infection

The retroviral expression vector, which encodes the double-stranded RNA corresponding to nucleotides 864–883 of the mouse CHIP coding region or to enhanced green fluorescent protein (EGFP), was constructed using pMX-puro, kindly provided by Dr Kitamura (Osaka University, Graduate School of Medicine, Osaka, Japan). For retrovirus-mediated gene expression, Neuro2A cells were infected with retroviruses produced by Plat-E packaging cells and then cultured in the presence of 0.2 μg/mL puromycin (Sigma). pMX-neo vector was used for Myc-tau (P301L).

Induction and detection of cell death

Stable Neuro2A cell lines were cultured with 20 μM MG132 (Peptide Institute, Osaka, Japan) and incubated for 24 h; the cell number was counted after trypan blue staining.

Immunohistotochemical staining

Brains were immersion fixed with 10% buffered formalin and paraffin-embedded sections (2–10 μm) were prepared for confocal microscopic analyses. Deparaffinized sections were treated in either 0.1% Triton X-100 in phosphate-buffered saline for 20 min or Target Retrieval Solution (Dako Cytomation Denmark A/S, Glostrop, Denmark). AT8 and anti-CHIP were used as primary antibodies and then incubated with either Alexa488/568-conjugated anti-mouse IgG or Alexa488/568-conjugated anti-rabbit IgG. Sections were then examined with a Radiance 2000 KR3 confocal microscope (Bio-Rad Laboratories, Hercules, CA, USA).

Results

We first examined the involvement of U-box proteins in tau ubiquitylation. The overexpression of UFD2a, UFD2b or PRP19 U-box proteins had no effect on tau ubiquitylation compared with control, which showed only minimal tau ubiquitylation with endogenous E3 ligases (Fig. 1a). Only CHIP overexpression exhibited poly-ubiquitylated tau (Fig. 1a), suggesting that CHIP participates in this ubiquitylation process. To confirm this result, various combinations of tau, Myc-CHIP and HA-tagged ubiquitin were expressed in COS7 cells and tau was purified from the heat-stable materials of each cell lysate by immunoprecipitation using an anti-tau antibody. Tau from Myc-CHIP- and HA-tagged ubiquitin-coexpressing cells revealed anti-HA immunoreactivity, suggesting that tau protein is covalently modified by ubiquitin under the expression of CHIP (Fig. 1b). This result was verified by purifying ubiquitylated protein from CHIP- and tau-expressing cells. Using an Ni column, ubiquitylated proteins were purified from cells expressing tau, histidine-tagged Ub with or without CHIP. CHIP expression greatly enhanced the recovery of ubiquitylated tau in elution fractions 1 and 2 (Fig. 1c) and the ubiquitylated tau by CHIP was about 3.4% of total tau. Thus, CHIP is an E3-ubiquitin ligase for tau and the overexpression of CHIP increases tau ubiquitylation in an *in vivo* system. To further confirm the ubiquitylation of tau by CHIP, we reconstituted ubiquitylated tau in an *in vitro* ubiquitylation assay with these recombinants; E1, E2 (UbcH5C), GST-ubiquitin (GST-Ub), GST-CHIP and His-tau were required for tau ubiquitylation (Fig. 1d). Unexpectedly, chaperone proteins, phosphorylated tau or other such factors were not required for tau ubiquitylation by CHIP. Thus, these results indicated that CHIP alone can ubiquitylate even non-phosphorylated tau *in vitro*.

To test the interaction between tau and CHIP *in vivo*, mutants with CHIP and tau deletions (Fig. 2) were prepared and expressed in HEK293 or COS7 cells. Full-length tau could bind to full-length CHIP but not to CHIP (ΔU) lacking a U-box domain, CHIP (ΔTPR) lacking a TPR or CHIP (ΔCU) lacking both the charged region and U-box (Fig. 2a). Conversely, full-length CHIP could associate with full-length tau (four-repeat) and with the region lacking the N-terminus of tau (R-C) but not with the region lacking the repeat regions (ΔR) (Fig. 2b). These findings suggest that CHIP associates with the microtubule-binding repeat regions of tau. We further investigated the interaction and ubiquitylation of CHIP on four- and three-repeat tau (Fig. 2c). Three-repeat tau was less efficiently ubiquitylated by CHIP (Fig. 2d) and the association of three-repeat tau and CHIP was much less than for four-repeat tau (Fig. 2c). Thus, CHIP might recognize around the second repeat region of tau, which corresponds to exon 10 and preferentially ubiquitylates four-repeat tau.

We next investigated the effects of CHIP on the stability of tau in Neuro2A cells stably expressing Myc-tau (P301L) and FLAG-CHIP (Fig. 3a). The stability of tau (P301L) was examined by cyclohexamide-chase analysis. After cycloheximide treatment, endogenous $p27^{Kip1}$ protein rapidly degraded (Fig. 3a, two blots from bottom) and endogenous HSP90 protein remained stable for over 30 h (Fig. 3a, third and

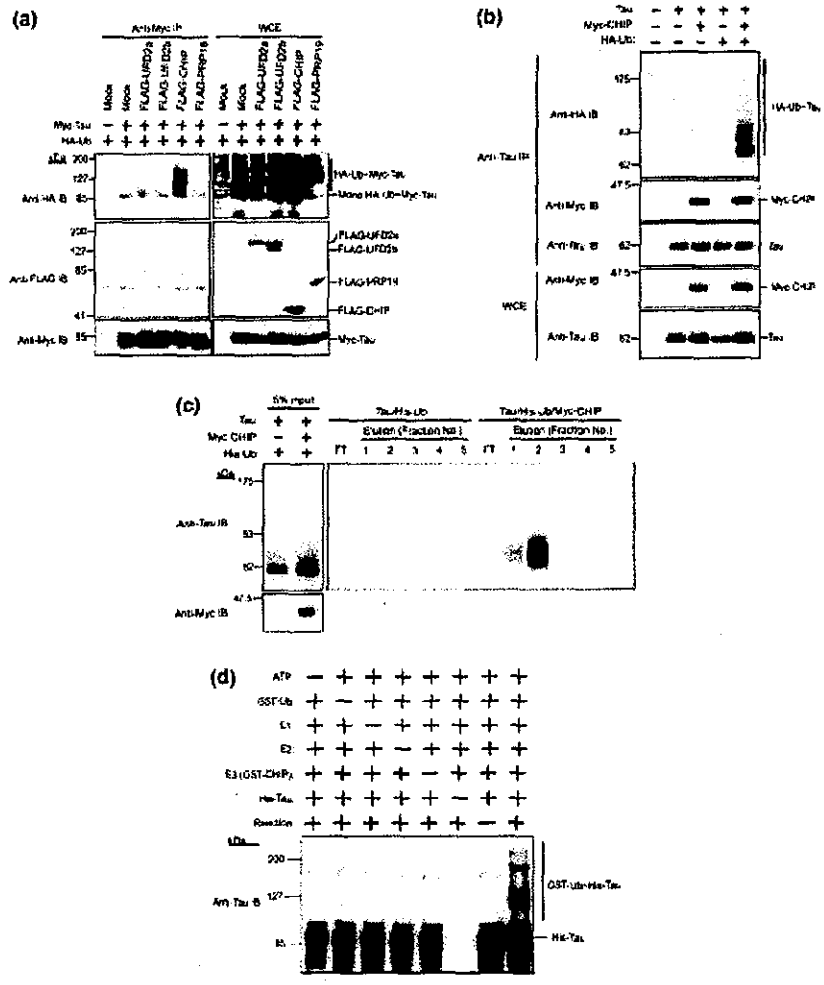

Fig. 1 Carboxyl terminus of Hsc70-interacting protein (CHIP) expression enhances the *ubiquitylation on tau in vivo*. (a) Specific ubiquitin ligase activity of CHIP for tau. The expression vectors for FLAG-UFD2a, *-UFD2b, -CHIP, -PRP19, Myc-tagged human four*-repeat tau and HA-tagged ubiquitin (HA-Ub) were transfected into HEK293T cells, the cell lysates were immunoprecipitated with anti-Myc monoclonal antibody and an anti-HA immunoblot was performed to detect the ubiquitylation on tau. Ten percent of cell lysates were used as WCE to detect the expression of each protein. (b) *In vivo* ubiquitylation assay for tau with CHIP. The expression vectors for Myc-CHIP, tau and HA-Ub were transfected into COS7 cells, the cell lysates were then immunoprecipitated with anti-tau monoclonal antibody and an anti-HA immunoblot was performed to detect the ubiquitylation on tau. Ten percent of cell lysates were used as WCE to detect the expression of each protein. (c) Fractionation of ubiquitylated tau from a cell expressing CHIP. The expression vectors for Myc-CHIP, tau and HA-Ub were transfected into COS7 cells, the cell lysates were then fractionated using an Ni column and an anti-tau immunoblot was performed to detect the ubiquitylation on tau. Five percent of cell lysates were used as WCE to detect the expression of each protein. (d) *In vitro* ubiquitylation assay for tau with CHIP. Each component [ATP, glutathione S-transferase (GST)-Ub, E1, Ubc4, GST-CHIP and His-tau] was mixed, incubated at 30°C for 2 h, subjected to sodium dodecyl sulfate–polyacrylamide gel electrophoresis and then immunoblotted with anti-tau monoclonal antibody. IB, immunoblot; IP, immunoprecipitate; WCE, whole cell lysate.

fourth blots from top) when CHIP and tau were overexpressed together (Fig. 3a, third and seventh blots) and when tau alone was overexpressed (Fig. 3a, fourth and eighth blots from the top). Tau remained stable for over 30 h only in cells overexpressing tau (Fig. 3a, first blot), whereas the overexpression of CHIP enhanced tau degradation (Fig. 3a, second blot) without changing the exogenous expression level of CHIP (Fig. 3a, sixth blot from top). Moreover, tau ubiquitylated by CHIP accumulated when treated with the proteasome inhibitor lactacystin (Fig. 3b) These results suggest that CHIP induces the ubiquitylation of tau which is followed by degradation via proteasome. The effects of CHIP on the stability and ubiquitination of tau were not different between the P301L mutant and wild tau.

Knowing that CHIP recognizes and ubiquitylates tau and that this is followed by proteasome degradation, we investigated the role of CHIP in SDS-insoluble tau formation, one of the biochemical features of paired

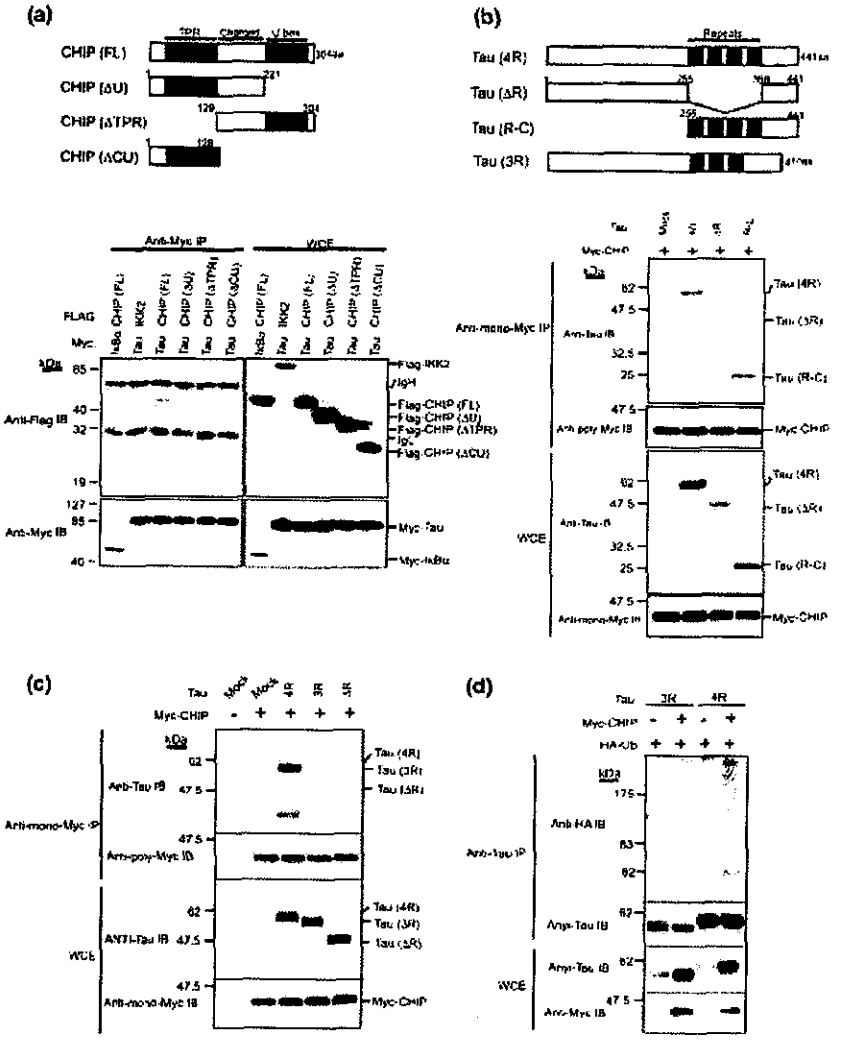

Fig. 2 Interaction between carboxyl terminus of Hsc70-interacting protein (CHIP) and four-repeat (4R) tau. (a) *In vivo* interaction between CHIP and tau. CHIP (FL) has the full-length (1–304) of CHIP. CHIP (ΔU), CHIP (ΔTPR) and CHIP (ΔCU) contain deletions of the U-box domain (222–304), tetratricopeptide repeat (TPR) domain (1–128) and charged region plus U-box domain (129–304), respectively. Black and gray boxes show the TPR and U-box domains, respectively. The expression vectors for full-length and mutants of FLAG-CHIP and Myc-tau (4R) were transfected into HEK293T cells, the cell lysates were immunoprecipitated with anti-Myc monoclonal antibody and anti-FLAG immunoblot was performed to detect the association with FLAG-CHIP or its mutants. Ten percent of cell lysates were used as WCE to detect the expression of each protein. Myc-IκBα and FLAG-IKK were used for negative controls. (b) Repeat domain of 4R tau interacts with CHIP. Tau (4R) is the longest form of 4R tau. Tau (ΔR) and tau (R-C) are the deletion of the 4R domain (256–441) and the N-terminal half (1–255), respectively. Black box shows repeat domain. The expression vectors for Myc-CHIP and truncated tau (4R) were transfected into COS7 cells, the cell lysates were immunoprecipitated with anti-Myc monoclonal antibody and anti-tau immunoblot was performed to detect the association with Myc-CHIP. The amount of immunoprecipitated CHIP was the same in all cell lysates (bottom panel). Ten percent of cell lysates were used as WCE to detect the expression of each protein. (c) Association of CHIP with 4R and three-repeat tau (3R). cDNAs described on the top of the blots were transfected into COS7 cells and cell lysates were immunoprecipitated using anti-myc antibody. Immunoprecipitants were probed by the anti-tau antibody TauC or anti-polyclonal antibody Myc. The amount of immunoprecipitated CHIP was the same in all cell lysates (bottom panel). (d) Ubiquitylation of 4R and 3R tau by CHIP. Each combination of cDNAs was transfected into COS7 cells. After immunoprecipitation of heat-stable materials using anti-tau antibody (HT7), immunoprecipitants were probed by anti-HA or tau C. The amount of immunoprecipitated tau was the same in all cell lysates (anti-tau IB panel in anti-tau IP panels) while the tau expression level was different.

helical filament-tau, using Neuro2A coexpressing frontotemporal dementia with parkinsonism-17 mutant tau (P301L) with or without FLAG-CHIP. The expression of P301L mutant tau induced the formation of SDS-insoluble tau and enhanced the recovery of tau in the SDS-insoluble fraction (formic acid-soluble fraction) by treatment with